# Nb$_2$O$_5$-Based Photocatalysts

*Kaiyi Su, Huifang Liu, Zhuyan Gao, Paolo Fornasiero,\* and Feng Wang\**

Photocatalysis is one potential solution to the energy and environmental crisis and greatly relies on the development of the catalysts. Niobium pentoxide (Nb$_2$O$_5$), a typically nontoxic metal oxide, is eco-friendly and exhibits strong oxidation ability, and has attracted considerable attention from researchers. Furthermore, unique Lewis acid sites (LASs) and Brønsted acid sites (BASs) are observed on Nb$_2$O$_5$ prepared by different methods. Herein, the recent advances in the synthesis and application of Nb$_2$O$_5$-based photocatalysts, including the pure Nb$_2$O$_5$, doped Nb$_2$O$_5$, metal species supported on Nb$_2$O$_5$, and other composited Nb$_2$O$_5$ catalysts, are summarized. An overview is provided for the role of size and crystalline phase, unsaturated Nb sites and oxygen vacancies, LASs and BASs, dopants and surface metal species, and heterojunction structure on the Nb$_2$O$_5$-based catalysts in photocatalysis. Finally, the challenges are also presented, which are possibly overcome by integrating the synthetic methodology, developing novel photoelectric characterization techniques, and a profound understanding of the local structure of Nb$_2$O$_5$.

## 1. Introduction

Abundant fossil resources are utilized to fulfill the growing energy and chemical requirements.[1] However, carbon dioxide generated in these processes is inevitably released into the environment, accompanying global warming, ocean acidification, and a

K. Su, Dr. H. Liu, Z. Gao, Prof. F. Wang
State Key Laboratory of Catalysis (SKLC)
Dalian National Laboratory for Clean Energy (DNL)
Dalian Institute of Chemical Physics (DICP)
Chinese Academy of Sciences
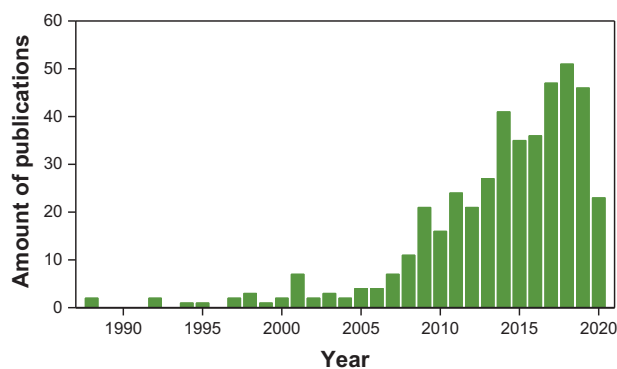Dalian 116023, China
E-mail: wangfeng@dicp.ac.cn
K. Su, Z. Gao
University of Chinese Academy of Sciences
Beijing 100049, China
Prof. P. Fornasiero
Department of Chemical and Pharmaceutical Sciences
INSTM - Trieste and ICCOM - CNR Trieste
University of Trieste
Via L. Giorgieri 1 Trieste 34127, Italy
E-mail: pfornasiero@units.it

series of ecological problems.[2] Moreover, the expected global energy consumption is up to 22.5 trillion watts (22.5 TW) of power demand in 2030.[3] Notably, electromagnetic radiation power flow from the Sun on the Earth is estimated to be 120 000 TW, which is far beyond the global energy consumption without carbon emission.[3] Learning from photosynthesis in nature, photocatalysis is potentially utilized for scalable and controlled production of fuel and diverse chemicals to alleviate the dependence on fossil fuels and the consequent environmental pollution.[4] Nowadays, diverse semiconductors are synthesized and applied in the photocatalytic process.[5] In principle, the electrons are motivated by the light and then transfer from valence band (VB) to conduction band (CB) in semiconductor photocatalysts, which induce subsequent redox reactions.[6] For instance, metal oxide, metal sulfide, metal nitride, metal phosphide, and nonmetallic material, like carbon nitride, are reported in the areas of photocatalysis, such as pollutant degradation, hydrogen generation, chemical synthesis, etc.[7] In these studies, researchers are devoted to preparing the photocatalysts that are nontoxic, eco-friendly, low-cost, and efficient, to realize reactions under mild conditions with massive desired products.

The niobium pentoxide (Nb$_2$O$_5$), a typically nontoxic solid oxide, exhibits strong redox ability and unique Lewis acid sites (LASs) and Brønsted acid sites (BASs).[4a,8] Previously, Ziolek's group and Tsang's group mentioned the photocatalytic performance of different niobium compounds and nanostructured Nb$_2$O$_5$ in 1999 and 2012, respectively.[4a,8a] Recently, the amount of publications in Nb$_2$O$_5$ photocatalyst increased rapidly over the past decade (**Figure 1**), indicating the novel discovery and profound understanding of Nb$_2$O$_5$. Concretely, the applications of Nb$_2$O$_5$ are extended to the photocatalytic conversion of waste plastics, activation of hydrocarbon, photoreduction of CO$_2$, and selective transformation of amines and alcohols.[9] For instance, Nb$_2$O$_5$ exhibited a higher reaction rate and selectivity than those of TiO$_2$ in the selective photooxidation of benzylamine to *N*-benzylidene benzylamine.[9c] Besides, inert polyethylene and waste plastics were completely degraded on Nb$_2$O$_5$ at 25 °C, while the generated CO$_2$ was further reduced to CH$_3$COOH.[9a] The selectivity of CO$_2$ to CO, CH$_4$, and other acid products is related to the distribution of LAS and BAS on the Nb$_2$O$_5$ surface.[9b] These results suggest the attractive properties of Nb$_2$O$_5$ and its potential in practical applications. However, a few review articles systematically summarize Nb$_2$O$_5$-based photocatalysts to provide the structure–activity relationship for future studies.

**Figure 1.** The amount of publications from the Web of Science by searching the keywords "Nb2O5" and "photocatal\*" on May 30, 2020.

Hence, we provide an overview of the recent advances in different $Nb_2O_5$-based photocatalysts, including the synthesis, application, and relationship between the photoelectronic properties, surface structures, and activities. First, the physicochemical properties of $Nb_2O_5$ are introduced. Then, reported $Nb_2O_5$-based photocatalysts are classified into two categories: i) pure $Nb_2O_5$ catalysts with diverse morphology, and ii) $Nb_2O_5$ catalysts with other species, such as metal species and other components. In the synthetic sections, we summarize the method and the role of treatment and additives in the control of morphology and structure. After that, we discuss the optical and catalytic properties of $Nb_2O_5$-based photocatalysts (**Figure 2**). Except for the generation, migration, and recombination of charge carriers, acidic properties and Nb–O–metal interface are also taken into account, which can affect the interaction between substrate molecules and catalyst, the product selectivity, and reaction rate. In the end, we give the summary and outlook of $Nb_2O_5$-based photocatalysts.

## 2. The Nature of $Nb_2O_5$

### 2.1. Resource

The abundance of niobium on earth is 20 ppm.[8a] Niobium does not exist in a pure metallic form but is often found as mixtures with other metals in minerals, which are unevenly distributed around the globe.[10] Abundant columbic mines are mainly located in Brazil, Canada, and Nigeria.[8a] Nowadays, niobium compounds are widely utilized in superconducting, electronics, and catalytic industries, indicating that the recovery of niobium-containing solid waste is potential strategies to produce desired niobium oxide.[11] In the field of catalysis, niobium powders and $Nb_2O_5$ obtained from the minerals are the raw material for the production of niobium chloride, niobium oxalate, ammonia niobium oxalate, niobium pentabutoxide, and other organic niobium salts, which can be utilized for further preparation of nanostructured $Nb_2O_5$ due to the differences in acidity, alkalinity, and solubility.[4a,8a,12]

### 2.2. Physicochemical Properties

The $Nb_2O_5$ is an n-type semiconductor.[13] The structure of $Nb_2O_5$ depends on the preparation conditions.[14] Amorphous $Nb_2O_5$ can be transformed into pseudohexagonal phase (TT-$Nb_2O_5$), orthorhombic phase (T-$Nb_2O_5$), and monoclinic phase (H-$Nb_2O_5$) by increasing the temperature.[8a] Unique properties are observed in $Nb_2O_5$. $Nb_2O_5$ has the bandgap energy ($E_g$) value of $\approx 3.0$–$3.4$ eV, which is suitable for redox reaction in photocatalysis.[4a] As shown in **Figure 3**a, the excited electrons and holes on $Nb_2O_5$ migrate to the surface under light irradiation and then interact with the substrate in the reduction process and oxidation process, respectively. Besides, LASs and BASs are observed on tetrahedral $NbO_4$ and octahedral $NbO_6$ units (Figure 3b,c), respectively.[14a,b,15] The $Nb_2O_5$ exhibits high acid strength and is utilized in the dehydration reaction, hydrolysis reaction, and hydrodeoxygenation reaction.[8a,16] Meanwhile, these structures can be distorted by decreasing the thickness of $Nb_2O_5$ and reduction with the formation of $Nb_2O_{5-x}$ and $NbO_2$.[15,17] In addition, $H_2O$ and hydroxyl groups on the $Nb_2O_5$ surface can be removed by post-treatment, resulting in the improvement of absorption performance.[18] Except for the unique acidity and redox properties, $Nb_2O_5$ is robust in organic acid solutions. This property implies that $Nb_2O_5$ can be stable in acidic solutions derived from biomass and other acid products in photocatalysis. However, there are still some limitations of $Nb_2O_5$. An unavoidable trade-off is present between the restricted optical absorption and suitable photoredox ability of $Nb_2O_5$. In addition, the methods are still necessary for the large-scale production of specific morphology of $Nb_2O_5$-based photocatalysts. Thus, an overview is conducive to the systematic understanding and development of $Nb_2O_5$-based photocatalysts.

## 3. Synthesis of $Nb_2O_5$-Based Photocatalysts

### 3.1. Synthesis of Pure $Nb_2O_5$ Catalysts

The specific surface area (SSA) of commercial $Nb_2O_5$ (orthorhombic phase) is lower than 15 $m^2$ $g^{-1}$.[17b] This property leads to the restricted active sites and a high recombination efficiency of charge carriers on $Nb_2O_5$.[20] Nowadays, the $Nb_2O_5$ catalysts with diverse morphologies are synthesized to solve these problems in photocatalysis.[8e] These catalysts can be divided into three classes: 1D, 2D, and 3D $Nb_2O_5$ catalysts. Although 0D $Nb_2O_5$ quantum dots (QDs) were synthesized by the physical vapor deposition, the application of $Nb_2O_5$ QDs in photocatalysis is rarely reported.[21] Therefore, the synthesis and applications of $Nb_2O_5$ QDs are not mentioned in this work.

### 3.1.1. 1D $Nb_2O_5$ Catalysts

Recently, diverse methods have been developed for the synthesis of 1D $Nb_2O_5$ nanorods, nanowires, and nanotubes. In 2006, the preparation of $Nb_2O_5$ nanotubes was reported by the atomic layer deposition (ALD) approach.[22] Amorphous $Nb_2O_5$ was deposited first on the porous $Al_2O_3$ template with gas pulses of niobium iodide ($NbI_5$) and oxygen.[22] Then, $Al_2O_3$ was removed by chromic acid/phosphoric acid solution to produce desired $Nb_2O_5$ nanotubes.[22] Because of the costly apparatus and low yield of catalysts in the ALD process, other synthesis methods are necessary. The 1D T-$Nb_2O_5$ and TT-$Nb_2O_5$ nanotubes were obtained

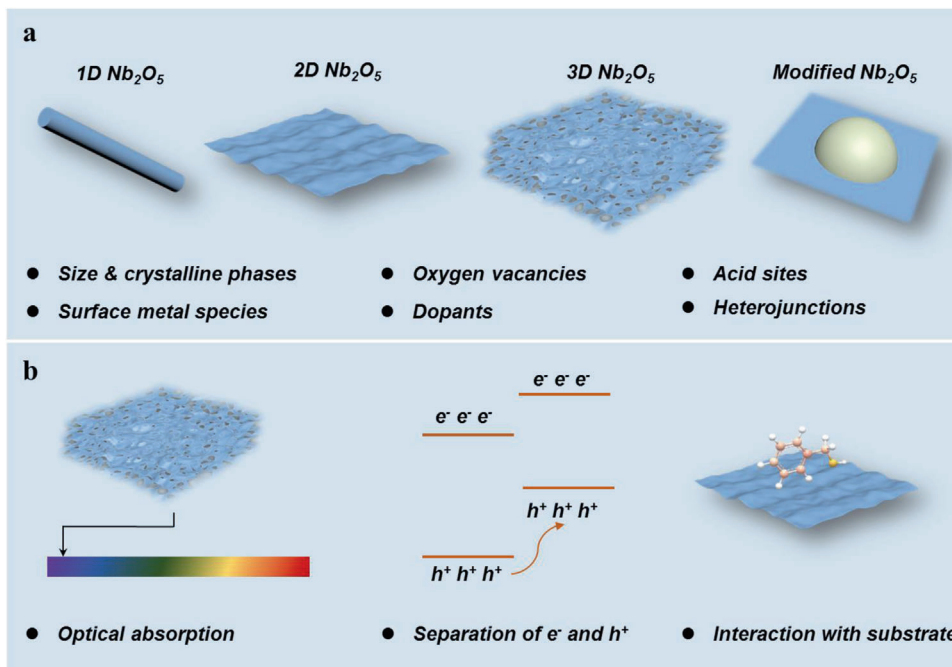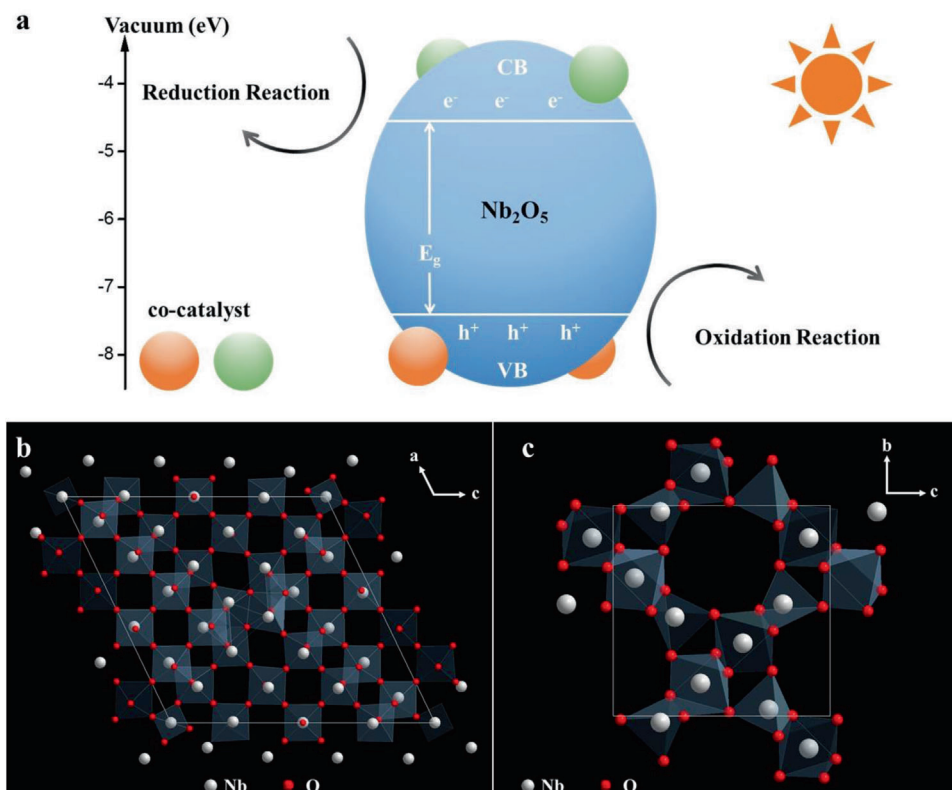**Figure 2.** An overview of a) $Nb_2O_5$-based photocatalysts and b) plausible influence in photocatalysis.



**Figure 3.** a) The photocatalytic process on $Nb_2O_5$, and the local structure of b) H-$Nb_2O_5$ and c) T-$Nb_2O_5$.[8a,19] a) Adapted with permission.[19] Copyright 2014, Royal Society of Chemistry. b,c) Adapted with permission.[8a] Copyright 1999, American Chemical Society.

**2003156 (3 of 25)**

**ADVANCED
SCIENCE NEWS**

www.advancedsciencenews.com

**ADVANCED
SCIENCE**

Open Access

www.advancedscience.com

from layered niobates.[23] First, layered $K_4Nb_6O_{17}$ was synthesized from the solid reaction of $Nb_2O_5$ and $K_2CO_3$ under the calcination. Then, the scrolled $H_4Nb_6O_{17}$ was prepared via the exfoliation of $K_4Nb_6O_{17}$ with the assistance of acid and base. Finally, the $Nb_2O_5$ nanotubes were obtained from $H_4Nb_6O_{17}$ by dehydration under 400–450 °C. The heat treatment was a vital process for the transformation of nanosheets to nanotubes.[23] Besides, the Kirkendall effect was applied in the synthesis of $H-Nb_2O_5$ nanotubes from nanorods by a two-step hydrothermal synthesis approach.[24] The $TT-Nb_2O_5$ nanorod arrays grew on niobium foils in the first hydrothermal process. Due to the Kirkendall effect, the outside walls of $TT-Nb_2O_5$ nanorods exhibited preferential nucleation and growth in the second hydrothermal process, which is accompanied by the migration of inside core composition and the formation of nanotubes. After that, a one-step hydrothermal method was reported.[25] The $Nb_2O_5$ powders, hydrofluoric acid (HF), hydrogen peroxide, and Ti powders were introduced into the precursor. Hydrofluoric acid acted as an etching reagent to disperse Nb powders in solution.[25,26] In addition, the evolution of nanotubes was significantly affected by the concentration of $F^-$ ions. This phenomenon may be due to the fact that $F^-$ anions act as a structure-directing agent to control the crystal growth.[25,26] Similarly, $T-Nb_2O_5$ nanotubes were obtained by the electrochemical method, which consisted of the anodization of Nb with ammonium fluoride.[27] However, toxic reagents (e.g., HF, $NH_4F$, or $H_2O_2$) are required in these processes.

Compared to the nanotubes, $Nb_2O_5$ nanorods can be synthesized directly from Nb probes and foils by a calcination method at $\approx 1000$ °C.[28] Besides, the decomposition of niobium isopropoxide was controlled to prepare the $Nb_2O_5$ nanorods in chemical vapor deposition (CVD) at 950 °C.[12d] The synthesis methods of $Nb_2O_5$ nanorods were reported at lower temperatures in other studies. For instance, $TT-Nb_2O_5$ nanorods encased in carbon were obtained from the niobium ethoxide by calcination at 800 °C in the 3 mL autoclave under nitrogen.[29] To remove the carbonaceous residues, the as-synthetic material was further treated at 500 °C under air condition, leading to the formation of $T-Nb_2O_5$ nanorods.[29] Besides, the topochemical method was developed, which is composed of the i) synthesis of specific morphology of niobates, ii) ion-exchange for removal of other metal ions on niobates, and iii) calcination for the phase transformation.[30] Typically, the $KNb_3O_8$ nanowires were prepared by molten salts of $Nb_2O_5$ and KCl under 800 °C and treated with $HNO_3$ to produce $H_3ONb_3O_8$ nanorods, which were further calcinated to produce the $H-Nb_2O_5$ nanorods.[30b] Similarly, $CaNb_2O_6$ nanowires were also utilized to prepare the $H_2Nb_2O_6$ nanorods, which were further transformed to produce the $T-Nb_2O_5$ nanorods.[31] Additionally, the solvothermal approach was reported in the catalyst preparation, following the calcination treatment to prepare the $Nb_2O_5$ nanorods from amorphous $Nb_2O_5 \cdot nH_2O$. The additives, like alcohol, played a key role in the hydrothermal process.[32] If alcohols are present in the solution, the $Nb_2O_5$ particles were observed. According to this phenomenon, $TT-Nb_2O_5$ nanorods were synthesized by a one-step alcohothermal method, which is contributed to the growth direction of [001] for the 1D structure under enough reaction time, temperature, and concentration of $NbCl_5$.[32] Likewise, $TT-Nb_2O_5$ nanorods were obtained by introducing oleic acid and trioctylamine, isopropanol, benzyl alcohol (BA), and triethylamine in the hydrothermal process.[12a,33] In ad-

dition, corrosive $NH_4F$ and $H_2O_2$, HF, cetyltrimethylammonium bromide, and ionic liquid are also effective additives.[34] Particularly, the rodlike structure was observed when the hydrothermal process was prolonged to 30 days without any additives.[35] Electrospinning was also utilized in the synthesis of $Nb_2O_5$ nanorods.[36] A mixture of $Nb(OEt)_5$, polyvinylpyrrolidone (PVP), acetic acid, and ethanol solution was prepared before the electrospinning. The complex of PVP and acetic acid in the solution acted as a template.[36] After electrospinning operation, the obtained material was treated at 550 °C to produce the $Nb_2O_5$ nanorods under air condition.[36] In these methods, calcination is generally utilized for the removal of carbonaceous impurities or the change in the crystallinity.
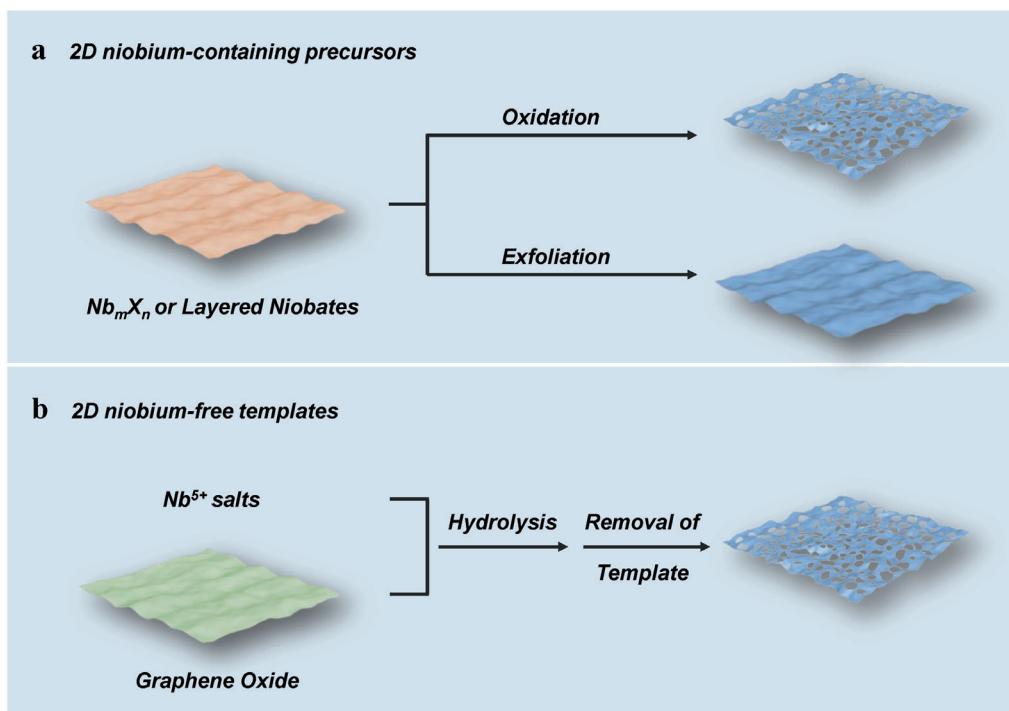
For the synthesis of $Nb_2O_5$ nanowires, a thermal oxidation approach was reported from the linear Nb foils under 900–1000 °C.[37] Similarly, $Nb_2O_5$ nanowires can be obtained from the topochemical method. $T-Nb_2O_5$ was synthesized from $NaNbO_3$ nanowires under 700 °C.[38] $H-Nb_2O_5$ nanowires were also prepared from $Nb_3O_7(OH)$ nanorods by calcination at 450 °C.[39] Besides, $TT-Nb_2O_5$ nanowires can be prepared with the assistance of reflux.[40] The refluxing is a useful approach to synthesize metal oxide nanorods with suitable additives for crystal growth, like trioctylamine, which directly affects the pH, the hydrolysis, and deposition of the precursor.[40] When the precursor solution tends to be acidic, high crystallinity of $Nb_2O_5$ nanowires is observed after calcination.[40] In addition, electrospinning was also reported in the preparation of $T-Nb_2O_5$ nanowires.[41] Furthermore, Nb foil was treated with oxygen plasma to induce the growth of $Nb_2O_5$ nanowires over the Nb foil.[42]

### 3.1.2. 2D $Nb_2O_5$ Catalysts

$Nb_2O_5$ nanosheets are typical 2D materials, which are attractive due to their unique structure and electronic properties. Previously, $Nb_2O_5$ nanosheets could be fabricated directly from the raw $Nb_2O_5$ and $NbCl_5$ without any templates or organic polymers.[43] For instance, $\approx 3$–5 nm $T-Nb_2O_5$ nanosheets were produced from commercial $NbO_2$ particles in a solution containing ethanol and urea under 130 °C for 30 days.[44] Similarly, $TT-Nb_2O_5$ nanosheets were also synthesized from $NbCl_5$ in ethylenediamine solution by hydrothermal treatment and calcination.[45] In this process, the alkaline additive may be beneficial for the nanosheet evolution.[46] Especially, Wang's group reported the synthesis of the $Nb_2O_5 \cdot xH_2O$ nanosheets from $NbCl_5$ by a one-step hydrothermal method and revealed the effect of additives.[47] They speculated that the alkaline $NH_3 \cdot H_2O$ may play a key role in nanosheet synthesis. To prove the opinion, they replaced the $NH_3 \cdot H_2O$ with other alkaline additives, like the NaOH, $n$-butyl amine, and $t$-butylammonium hydroxide (TBAOH).[47] Nanosheetlike morphology is only obtained using $n$-butyl amine and TBAOH, suggesting the vital role of the $NH_4^+$ ions. The ions in the $Nb_2O_5$ nanosheets, like $NbO_4^{3-}$, $NbO_5^{5-}$, and $NbO_6^{7-}$, exhibit negative charges, which show an electrostatic interaction with $NH_4^+$ ions that act as a capping agent. This interaction can restrain the interlamination growth and avoid the formation of bulk $Nb_2O_5$.[47]

In addition to $NbO_2$ and $NbCl_5$, other 2D columbic compounds are also applied in the synthesis of $Nb_2O_5$ nanosheets by

**ADVANCED
SCIENCE NEWS**

www.advancedsciencenews.com

**ADVANCED
SCIENCE**
Open Access

www.advancedscience.com

**Figure 4.** Synthesis of $Nb_2O_5$ nanosheets with the assistance of 2D a) niobium-containing precursors and b) niobium-free templates.

the topochemical method (**Figure 4**a). For instance, 2D $Nb_mX_n$ (X = Se and S) materials were utilized to prepare the $Nb_2O_5$ nanosheets.[48] The $Nb^{4+}$ species in $NbSe_2$ oxidized to $Nb^{5+}$ ions with the formation of Se under calcination, leading to the generation of porous $Nb_2O_5$ nanosheet.[48] Besides, the $Nb_3O_7F$ nanosheets were produced by a hydrothermal approach and further calcinated to prepare the T-$Nb_2O_5$ nanosheets.[49] Additionally, other niobates were also reported in the synthesis of $Nb_2O_5$ nanosheets.[17c,50] For instance, layered $KNb_3O_8$ was prepared by calcination of commercial $Nb_2O_5$ and $K_2CO_3$.[17c] After that, the layered $HNb_3O_8$ was obtained from the $KNb_3O_8$ in an acidic solution by ion-exchange.[17c] Ultimately, few-layer $HNb_3O_8$ nanosheets were observed by the intercalation of TBAOH.[17c] Similarly, T-$Nb_2O_5$ nanosheets were obtained from the layered $H_4Nb_6O_{17}·3H_2O$.[51]

Besides, layered templates are applied in the synthesis of $Nb_2O_5$ nanosheets (Figure 4b). The graphene oxide (GO), a typical 2D material, was introduced into the cyclohexane solution, following the addition of $Nb(OC_4H_9)_5$.[52] After the hydrothermal process, $NbO_x$/GO nanosheets were observed.[52] Subsequently, ≈2–4 nm $Nb_2O_5$ nanosheets were obtained by the removal of GO under calcination.[52] Moreover, when the calcination temperature was elevated to 750 °C, holey T-$Nb_2O_5$ nanosheets were observed by the utilization of GO.[53] Likewise, silica/graphene nanosheets were utilized to prepare T-$Nb_2O_5$ nanosheets by the hydrolysis of $NbCl_5$.[54] The silica in the template was removed by NaOH, maintaining the porous structure of $Nb_2O_5$.[54] These preparation methods of $Nb_2O_5$ nanosheets can be divided into two classes. One kind of method is to synthesize layered intermediate that contains niobium to prepare nanosheets. Another

one is to afford 2D templates that are niobium-free to induce the growth of $Nb_2O_5$ nanosheets.

Furthermore, 2D ordered porous $Nb_2O_5$ were prepared with the assistance of chain ligand.[55] In 1996, Ying's group put forward a method to synthesize the mesoporous $Nb_2O_5$ molecular sieve with the assistance of ligands.[55] In this approach, $Nb(OEt)_5$ and tetradecylamine were utilized to produce ringed $Nb_2O_5$ via hydrolysis, which is controlled precisely by the volume of water, hydrolysis temperature, and time.[55] Because of the interaction between the basic amine ligand and $Nb_2O_5$, the residual tetradecylamine molecules were further removed by strong acid $HNO_3$/EtOH.[55] After that, block-copolymer/inorganic-salt methodology was developed.[56] The tetradecylamine can be replaced by poly (alkylene oxide) block copolymer, such as P-123.[56] Meanwhile, inorganic niobium salts, $NbCl_5$, were also utilized as a precursor in an ethanol solution.[56] The ordered mesoporous $Nb_2O_5$ was obtained by the formation of crown-ether-type complexes between alkylene oxide segments and inorganic ions through weak coordination bonds.[56] Especially, when inorganic Nb salts and aqueous solution were introduced simultaneously into the precursor with controlled hydrolysis, 3D mesoporous $Nb_2O_5$ were observed.[57] In addition to the utilization of a single hydrophilic ligand, amphiphilic block copolymers were also developed to fabricate $Nb_2O_5$ materials. The poly(ethylene-co-butylene)-b-poly(ethylene oxide) diblock copolymers were mixed with $NbCl_5$ in the ethanol solution, following the calcination to remove the polymers and obtain the 2D mesoporous $Nb_2O_5$.[58] The orientation of porous structure can be regulated by the changes in polymer hydrophilicity and hydrophobicity.[59] For instance, the polymers with different chain lengths, like

amphiphilic L64, P85, and P103, were effective in the synthesis of porous $Nb_2O_5$.[59]

### 3.1.3. 3D Nb₂O₅ Catalysts

Generally, the porous structure is beneficial for the diffusion and transmission of substrates.[60] Although the porous $Nb_2O_5$, HY-340, is supplied from the CBMM (Brazil, one commercial company), many research groups are still devoted to designing and developing novel synthetic methods of 3D porous $Nb_2O_5$ catalysts.

To date, 3D porous $Nb_2O_5$ catalysts can be synthesized from the Nb foils, niobium salts, and raw $Nb_2O_5$. The Nb foils were irradiated within a constant flux of 100 eV $He^+$ ions under 500–950 °C to prepare the porous $Nb_2O_5$.[61] With the increase of temperature, the pore diameter over $Nb_2O_5$ was larger, which can be up to 230 nm.[61] In addition, $Nb(OH)_5$ was obtained by the anodization of Nb foil in ethylene glycol containing 4 vol% HF and 2 vol% $H_2O_2$. Then, mesoporous $Nb_2O_5$ was obtained by the calcination of $Nb(OH)_5$.[62] In the anodization process, the porous structure was controlled by the changes in voltage, electrolyte temperature, time, and solution.[17d,62,63] Particularly, a careful cleaning process is necessary to remove the impurity on the surface of Nb foils before anodization.[63d] Besides, the sol–gel approach was also reported. $Nb(OC_2H_5)_5$ was hydrolyzed with the assistance of the $NH_3 \cdot H_2O$ solution and calcined at 300 and 650 °C to $TT-Nb_2O_5$ and $T-Nb_2O_5$, respectively.[64] Similarly, wormhole-like amorphous $Nb_2O_5$ and hierarchically porous $Nb_2O_5$ were prepared from the hydrolysis of Nb salts ($NbCl_5$ and $Nb(OC_2H_5)_5$) by the addition of P-123 and surfactant (Brij 56), respectively.[20,65] Other uniform templates, like polystyrene spheres and zeolites, were also utilized to prepare the porous $Nb_2O_5$. For instance, polystyrene spheres were introduced into the Nb–citric complex solution via the reaction of $Nb_2O_5$ with HF, $NH_3 \cdot H_2O$, and citric acid.[66] The template was subsequently removed by the calcination with the formation of macroporous $Nb_2O_5$.[66] The macropores size of $Nb_2O_5$ was greatly dependent on the diameter of the polystyrene spheres. Similarly, the ammonium niobate oxalate was deposited on the FDU-1, one type of zeolite, by an impregnation method.[67] Then, the FDU-1 is removed by a diluted NaOH solution. Furthermore, $T-Nb_2O_5$ and $TT-Nb_2O_5$ were obtained with the assistance of other porous carbon materials, such as cotton.[68] In these methods, the evolution of ordered porous structure mainly depended on the hydrolysis of niobium salt and the uniformity of templates.[57]

Porous $Nb_2O_5$ constituted by stacked particles was also reported.[69] For instance, $T-Nb_2O_5$ can be prepared by direct calcination of Nb powders.[69] In addition, the hydrolysis of organic Nb salts was also applied in the synthesis of nanoparticles. Especially, $Nb(OBu)_5$ was dissolved in toluene with different amounts of water in an autoclave under 300 °C for 2 h.[70] When the amount of water was up to 30 $cm^3$, amorphous $Nb_2O_5$ were transformed to TT-phase and grew from ≈5 to 30–60 nm, indicating that water was beneficial for the dissolution–recrystallization process on the growth of Nb–O–Nb structure.[70] Instead of toluene, ethanol, triethylamine, and $H_2O_2$ solution were also applied in the synthesis of $Nb_2O_5$ particles.[71] Besides, the $NbCl_5$ and Nb-fluoro complex were used in the synthesis of

$H-Nb_2O_5$ and $TT-Nb_2O_5$ particles, respectively.[72] In the hydrolysis process, structure-directing agents were introduced, such as the lauryl amine hydrochloride and F127.[73] The smaller particles of $Nb_2O_5$ were observed with the increase of pH.[74] Furthermore, other methods were developed for the synthesis of $Nb_2O_5$ particles. For instance, the supercritical-$CO_2$-assisted approach was introduced into catalyst preparation.[75] The hydrolyzed mixture of $NbCl_5$ dissolved in ethanol solution and aged in the supercritical $CO_2$ under 80 °C for 3 h. After the calcination under 200 °C, amorphous $Nb_2O_5$ particles with a high surface area (≈340 $m^2$ $g^{-1}$) were obtained.[75] In addition, the ball-milling process was reported for the low-temperature synthesis. Mixed $Nb_2O_5$ and $Na_2CO_3$ were formed by the reaction of $NbCl_5$ and $Na_2CO_3$.[76] The molar ratio of $NbCl_5$ to $Na_2CO_3$ and calcination temperature were controlled to inhibit the generation of unwanted niobates.[76] The additives, such as urea and melamine, acted as the fuel and template to fabricate $TT-Nb_2O_5$ particles in the calcination process.[12b,77] Furthermore, the as-synthesized $H-Nb_2O_5$ particles can be treated under laser pulses to prepare amorphous $Nb_2O_5$, $T-Nb_2O_5$, and $TT-Nb_2O_5$, realizing the reversible transformation of crystal structures.[78]

Other morphologies of $Nb_2O_5$ catalysts were also reported, such as the bulk, octahedron, hollow structure, and others.[79] The synthetic methods of these morphologies were partly similar to that of $Nb_2O_5$ particles under different conditions. For instance, the $Nb_2O_5$ particles can be further calcinated to prepare the bulk counterpart.[75] Besides, the resorcinol, formaldehyde, and ammonium niobate oxalate were utilized in the hydrothermal process for the synthesis of $Nb_2O_5$@polymer materials, which were further calcinated to remove the polymer and obtain the hollow $Nb_2O_5$ microspheres.[80]

## 3.2. Synthesis of Nb₂O₅ Catalysts with Other Species

### 3.2.1. Doped Nb₂O₅ Catalysts

Because of the wide bandgap of $Nb_2O_5$ (≈3.0-3.4 eV), the strategies by introducing doped atoms are applied to enhance the optical absorption ability, which was confirmed by experiments and first-principles calculations.[81] The synthetic methodologies can be classified into two approaches: a) synthesis from the mixture of additives and columbic precursors, and b) post-treatment of as-synthesized $Nb_2O_5$ catalysts (**Figure 5**). For instance, ethanol and acetic acid acted as the carbon sources and the solvent to prepare the carbon-doped $Nb_2O_5$ ($C–Nb_2O_5$) in the solvothermal process (Figure 5, path I).[82] Similarly, the niobium ethoxide and $NbCl_5$ were dispersed in a mixed solution of alcohol and nitrogenous additives in the solvothermal process, leading to the formation of nitrogen-doped $Nb_2O_5$ ($N–Nb_2O_5$).[33b,83] Besides, $N–Nb_2O_5$ can be obtained from the calcination of niobium salts with urea, melamine, and ammonium chloride.[12b,84] A series of rare-earth (Er, Eu, Pr, Tm, and Yb), Ag, Fe, Mo, Pd, Sr, W, Y, Zn, and Zr doped $Nb_2O_5$ materials were also synthesized from the calcination of mixing the niobium salts with other metal additives.[77,85] Additionally, the alkali metal doped $Nb_2O_5$ materials were also fabricated by the electrochemical approach. The Nb foils were oxidized at a pulsed current while the alkali metal ions in the
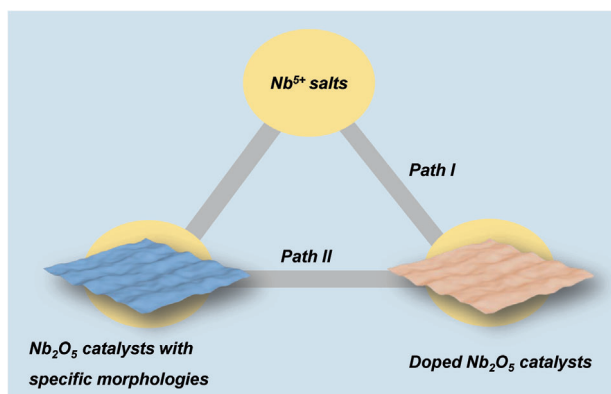
**ADVANCED**
**SCIENCE NEWS**
www.advancedsciencenews.com

**ADVANCED**
**SCIENCE**
Open Access
www.advancedscience.com

**Figure 5.** The synthesis of doped $Nb_2O_5$ catalysts.



**Figure 6.** The synthesis of composited $Nb_2O_5$ catalysts.

electrolytes were feasible to interact with $NbO_x$, resulting in the generation of M–$Nb_2O_5$ (M = Li, Na, K, Rb, and Cs).[86]

Moreover, as-synthesized $Nb_2O_5$ can be further treated (Figure 5, path II). Mesoporous $Nb_2O_5$ and citric acid were utilized to synthesize the C–$Nb_2O_5$ under the calcination at 400 °C.[73] The $Nb_2O_5$ was treated with $NH_3$ gas to prepare N–$Nb_2O_5$ under 400–600 °C.[87] In addition, the N–$Nb_2O_5$ was also synthesized from the calcination of porous $Nb_2O_5$ with urea.[19,50f,88] If urea is replaced by thiourea, the generation of sulfur-doped $Nb_2O_5$ (S–$Nb_2O_5$) can be observed.[73] Furthermore, N, S codoped $Nb_2O_5$ was obtained when the ratio of thiourea to $Nb_2O_5$ increased from 0.37 to 1.[89] Other metal atoms, like Mo atoms, can be introduced into the $Nb_2O_5$ lattices, which were synthesized from the hydrothermal process of ultrathin $Nb_2O_5$ nanosheets and ammonium molybdate.[90]

### 3.2.2. Metal Species Supported on $Nb_2O_5$ ($M/Nb_2O_5$) Catalysts

Diverse metals, metal oxides, and metal salts are utilized in the synthesis of $M/Nb_2O_5$. For instance, Pt and $Ag_2O$ powders were mixed with $Nb_2O_5$ to prepare the $Pt/Nb_2O_5$ and $Ag/Nb_2O_5$, respectively.[91] Accompanied by the development in nanotechnology, the size of metal particles was precisely controlled by the colloidal method, which can be further applied in the synthesis of $M/Nb_2O_5$.[48,92] For instance, ≈7.0 nm Pd nanoparticles were protected by the ligand, oleylamine, or oleic acid and introduced into the $Nb_2O_5$ suspension with the assistance of hexanes. The ligands on the Pd species can be further removed by calcination.[92d]

Metal salts were applied in the synthesis of $M/Nb_2O_5$ by the wet chemistry methods.[93] The $Au/Nb_2O_5$, $Ir/Nb_2O_5$, $Rh/Nb_2O_5$, $Ru/Nb_2O_5$, $Pd/Nb_2O_5$, and $Pt/Nb_2O_5$ were synthesized by the incipient wetness impregnation method.[93] The heteroatoms in the precursor, such as nitrogen and chlorine atoms, are reasonably removed by the calcination process.[93a] Whereas, the aggregation of metal species to nanoparticles was observed, ascribed to the heat treatment. The deposition–precipitation method was also developed to produce $M/Nb_2O_5$, following the calcination under lower temperature (≈300 °C).[8c] In the preparation of catalysts, $Au^{3+}$ ions were deposited on the $Nb_2O_5$ surface with the assistance of urea or ammonium hydroxide. The average diameter of Au nanoparticles was ≈5 nm after calcination.[8c] The $H_2$ can be replaced by $NaBH_4$ or hydrazine, which is an effective
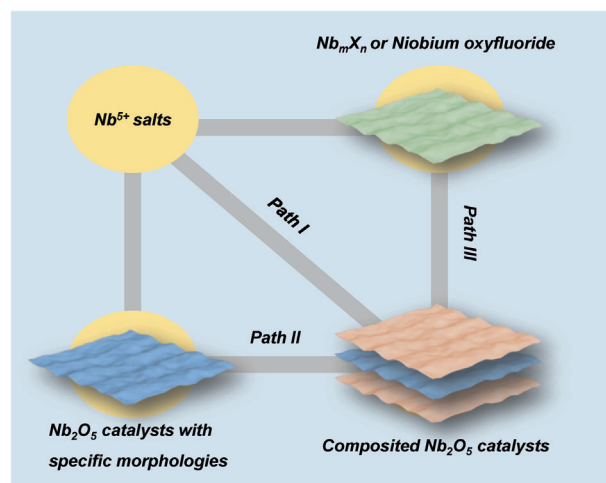
reductant for $RuCl_3$ and $Pd(acac)_2$ to $Ru/Nb_2O_5$ and $Pd/Nb_2O_5$ without heat treatment.[94] Instead of $NaBH_4$ and hydrazine, the reductive electrons can be directly generated from $Nb_2O_5$ under UV light irradiation.[4a] The $Au/Nb_2O_5$, $Pt/Nb_2O_5$, and $Pd/Nb_2O_5$ were fabricated by this approach.[95] Meanwhile, the photogenerated holes were captured by sacrificial agents, such as ethanol or isopropanol.[95] Besides, the electrostatic adsorption was available to prepare the highly dispersed metal nanoparticles supported on $Nb_2O_5$ under room temperature, attributed to the difference in point of zero charges (PZCs) between the metal ions and $Nb_2O_5$ at the same pH. Thus, $Ag/Nb_2O_5$ can be synthesized via the interaction between the $Ag(NH_3)_2^+$ and $Nb_2O_5$ at high pH (>5).[96]

### 3.2.3. Composited $Nb_2O_5$ Catalysts

The $Nb_2O_5$ can be modified by other metal oxides, metal sulfides, metal carbides, carbon materials, carbon nitride (g-$C_3N_4$), and black phosphorus (BP) to enhance its activity.[13,97] As-prepared $Nb_2O_5$, $NbC_2$, $Nb_3O_7F$, and niobium salts were reported in the synthesis of composited $Nb_2O_5$ catalysts (**Figure 6**).

Different Nb salts were reported in the synthesis of composited $Nb_2O_5$ photocatalysts (Figure 6, path I).[98] The methods mentioned in the preparation of pure phase $Nb_2O_5$ were also applied in the composited $Nb_2O_5$ photocatalysts. For instance, the CVD method was utilized to fabricate $Nb_2O_5/SiO_2$.[98] Besides, Nb precursors, like $NbCl_5$, and other metal salts were cohydrolyzed and precipitated to prepare mixed metal oxide particles.[99] Especially, ≈25–51 nm $Nb_2O_5$ nanocrystals were observed on the surface of ZnO nanorods, while ≈3–5 nm $Nb_2O_5$ microspheres were fabricated on the g-$C_3N_4$.[99e,g] This phenomenon can be ascribed to P123, which were conducive to the stabilization and dispersion of Nb micelles in the synthesis of $Nb_2O_5$/g-$C_3N_4$.[99g]

In addition, as-prepared $Nb_2O_5$ can be ground directly with $TiO_2$, $SrNb_2O_6$, $Bi_2O_3$, and GO to prepare the $TiO_2/Nb_2O_5$, $SrNb_2O_6/Nb_2O_5$, and $GO/Bi_2O_3/Nb_2O_5$, respectively.[100] Further calcination was conducted to improve the interaction between the $Nb_2O_5$ and other components (Figure 6, path II).[101] Besides, as-prepared $Nb_2O_5$ was also dispersed in solutions, such as isopropanol or tetrahydrofuran, to enhance the contact with

the $TiO_2$, BP, and $C_{60}$.[97c,102] In addition, the metal salt precursors were introduced into $Nb_2O_5$ suspension instead of as-synthesized metal oxide or metal sulfide.[103] The $ZnO/Nb_2O_5$ and $CdS/Nb_2O_5$ were prepared from $Zn(NO_3)_2$ and $CdCl_2$ by the impregnation approach, respectively.[104] The metal precursors, like $TiCl_4$, were hydrolyzed by the addition of $NH_3·H_2O$ and deposited on the $Nb_2O_5$ to obtain the $TiO_2/Nb_2O_5$.[103a] Besides, $CdS/Nb_2O_5/N$-GO was obtained from $Nb_2O_5$ by the deposition of CdS in the hydrothermal process. Especially, electrostatic adsorption was also reported to fabricate composited $Nb_2O_5$ catalysts.[13,105] In principle, the PZC can be utilized to screen materials that exhibit positive or negative surface charges, which are opposite to that on the $Nb_2O_5$ surface at the same pH value. Fortunately, $SiO_2$ and $g-C_3N_4$ as the potential candidates were reported.[13,105] Positive charges originated from amino groups that were exposed on the $g-C_3N_4$ surface in a pH range of 3–4. Meanwhile, the $Nb_2O_5$ surface is electronegative, ascribed to the presence of surface hydroxyl groups.[13] Compared to the impregnation approach, this method is available to prepare highly dispersed components on $Nb_2O_5$, due to the adsorption equilibrium. Excess $g-C_3N_4$ are possibly removed by washing and filtration, which differ from the drying treatment in the impregnation approach.[13] Furthermore, isolated species on $Nb_2O_5$ may be obtained by this method with precise control of precursor concentration, pH, and temperature.

Additionally, as-synthesized $NbC_2$ and $Nb_3O_7F$ were also utilized to prepare corresponding $Nb_2O_5$-based catalysts (Figure 6, path III). The $Nb_2O_5/C/Nb_2C$ and $Nb_3O_7F/Nb_2O_5$ photocatalysts were obtained by one-step calcination.[97d,106] The formation of $Nb_3O_7F/Nb_2O_5$ was ascribed to the decomposition of $Nb_3O_7F$ to $Nb_2O_5$ when the temperature is higher than 400 °C.[106] Similarly, the observed $Nb_2O_5$ supported on $Nb_2C$ was due to the reaction between $Nb_2C$ and $CO_2$ under 850 °C.[97d] Considering the thermal reaction, a series of composited photocatalysts with different $Nb_2O_5$ fractions are feasibly prepared, using the $Nb_2C$, NbN, $NbSe_2$, $NbS_2$, and $Nb_3O_7F$.[107]

## 4. Application of $Nb_2O_5$-Based Photocatalysts

### 4.1. Photodegradation of Pollutants

Nowadays, $Nb_2O_5$-based photocatalysts were widely reported in the photocatalytic photodegradation of pollutants (**Table 1**).[108] The hydrocarbons and chlorinated hydrocarbons (Table 1, Nos. 1–5), phenols (Table 1, Nos. 6–16), aldehydes (Table 1, No. 17), organic acids (Table 1, Nos. 18–26), ester (Table 1, No. 27), organic dyes, and pesticides (Table 1, No. 28–145) are oxidized on $Nb_2O_5$-based photocatalysts.[77,92b,109] In these processes, the wavelength ($\lambda$) of light sources is vital in photocatalysis, due to the limited absorption edge of photocatalysts.[8e] For instance, pure $Nb_2O_5$ exhibits large $E_g$ and is active under UV light irradiation ($\lambda <$ 400 nm).[4a] Accordingly, the black lamp, Xe lamp, and Hg lamp are available light sources.[108,110] Considering that ≈4% of the total solar spectrum is UV fraction, the strategies were developed to enhance the utilization efficiency of sunlight.[8e] Catalyst modification by dopant, surface metal species, and other semiconductors were useful to extend the optical absorption edge of $Nb_2O_5$.[5b] Thus, photodegradation of pollutants were also reported over $Nb_2O_5$-based photocatalysts under visible light irradi-
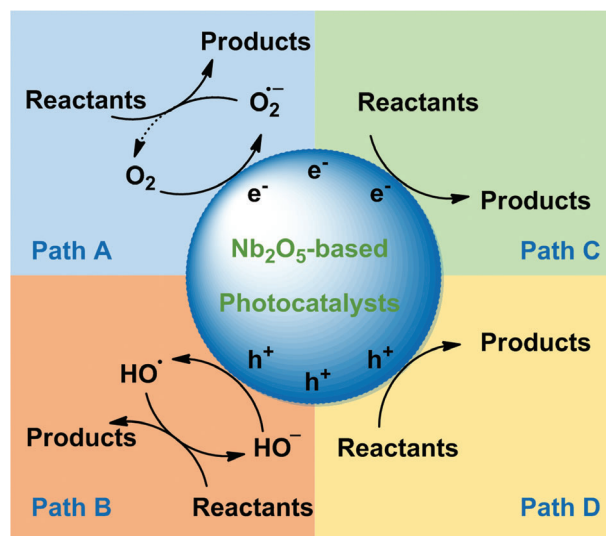


**Figure 7.** Possible reaction pathways over $Nb_2O_5$-based photocatalysts.

ation from other sources, including the fluorescent lamps, halide lamp, white LEDs, solar simulator, and sunlight.[77,99e,109b,111] In these processes, the ultraviolet filter can be utilized to eliminate the effect of UV light. Especially, the degradation of RhB was driven under visible light over pure $Nb_2O_5$ without the limitation of its bandgap energy (Table 1, No. 101). This process is ascribed to the dye-sensitized photocatalysis, in which the RhB molecules adsorbed on the $Nb_2O_5$ surface are excited by 440 nm light irradiation.[109e,112] The electrons transfer from the highest occupied molecular orbital (HOMO) to lowest unoccupied molecular orbital (LUMO) of RhB molecules and inject into the $Nb_2O_5$ conduction band, which induce the generation of active species for the succedent mineralization of the organic pollutant.[112]

Furthermore, the photodegradation of textile wastewater, palm oil mill effluent, petrol station wastewater, and vinasse was also reported (Table 1, Nos. 146–155).[113] These results suggested the potential of $Nb_2O_5$-based photocatalysts in practical applications. In these processes, the efficiency of catalysts is important in photocatalytic performance.[5b] Generally, the degradation rate is a common criterion for the comparison of activity (Table 1). However, the degradation rate is related to the ratio of the moles of organic pollutants to the mass of catalyst, temperature, and intensity of the light source. For instance, a change of reaction temperature is beneficial to the separation of photogenerated electrons and holes.[114] Increasing the intensity of the light source can improve the number of incident photons to enhance the reaction rate.[115] Thus, it is a complicated and difficult process for the comparison of the activity results. The utilization of photogenerated electrons and holes over $Nb_2O_5$-based photocatalysts can be used as another one criterion for the comparison of their activity. The organic pollutants can be degraded by the superoxide anions ($\bullet O_2^-$), hydroxyl radicals ($\bullet OH$), and photogenerated holes ($h^+$), corresponding to the path A, path B, and path D in **Figure 7**.[13,116] Therefore, the efficiency of electrons can be calculated by the ratio of products to the pollutants. However, the qualitative and quantitative analysis of obtained products is not always mentioned in the literature, leading to challenges in the

**Table 1.** Recent advances in the photodegradation of pollutants over $Nb_2O_5$-based photocatalysts.

| No. | Catalysts | Pollutants | Light sources | Reaction temperature [°C] | Degradation rate | Refs. |
|---|---|---|---|---|---|---|
| 1 | N-TiO$_2$–Nb$_2$O$_5$ | Benzene, toluene, and xylene | 46 W black lamp | 25 | 10 min$^{-1}$ | [108] |
| 2 | N–Nb$_2$O$_5$ | Toluene | Xe lamp | n.m.$^{a)}$ | ≈10% (60 min) | [110a] |
| 3 | Pt/Nb$_2$O$_5$ | Ethylene | Xe lamp | n.m. | 0.94 min$^{-1}$ | [95c] |
| 4 | T-Nb$_2$O$_5$ nanotubes | Trichloro-ethylene | UV light | n.m. | 100% (15 min) | [23c] |
| 5 | Nb$_2$O$_5$/TiO$_2$ | 1,4-dichlorobenzene | 150 W Xe lamp | n.m. | ≈60% (10 min) | [118] |
| 6 | TT-Nb$_2$O$_5$ particles | 2-chlorophenol | 400 W halide lamp (350–700 nm) | 30 | 0.13 h$^{-1}$ | [77] |
| 7 | Nb$_2$O$_5$ nanorods/graphene | 4-chlorophenol | 300 W Xe lamp (420–780 nm) | n.m. | ≈95% (210 min) | [119] |
| 8 | Carbon xerogel/Nb$_2$O$_5$/TiO$_2$ | 4-chlorophenol | 300 W lamp | 25 | 0.0078 min$^{-1}$ | [120] |
| 9 | WO$_3$/Nb$_2$O$_5$ | 4-nitrophenol | 125 W Hg lamp | 27 | 4.6 s$^{-1}$ | [121] |
| 10 | CeO$_2$/Nb$_2$O$_5$ | Phenol | UV light | n.m. | 90% (150 min) | [122] |
| 11 | Nb$_2$O$_5$ | Phenol | UV light | n.m. | 14% (15 min) | [123] |
| 12 | Nb$_2$O$_5$–Pr$_6$O$_{11}$ | Phenol | 6 W Hg lamp | n.m. | 2.5 × 10$^{-6}$ M s$^{-1}$ | [124] |
| 13 | Nb$_2$O$_5$–ZnS | Phenol | 8 W Hg lamp | n.m. | 58% (15 min) | [125] |
| 14 | Nb$_2$O$_5$/ZnO rods | Phenol | Sunlight | n.m. | 100% (40 min) | [99e] |
| 15 | Nb$_2$O$_5$/ZnO | Phenol | 15 W Hg lamp | n.m. | 100% (60 min) | [110b] |
| 16 | Sr–Nb$_2$O$_5$ | 2-chlorophenol | 400 W halide lamp (350–700 nm) | 30 | 0.58 h$^{-1}$ | [77] |
| 17 | Nb$_2$O$_5$–TiO$_2$ | Acetaldehyde | Xe lamp (350–700 nm) | r.t.$^{b)}$ | 0.0139 min$^{-1}$ | [126] |
| 18 | Amorphous Nb$_2$O$_5$ particles | Acetic acid | 400 W Hg lamp ($\lambda > 300$ nm) | 25 | 53 μmol h$^{-1}$ g$^{-1}$ | [70] |
| 19 | Pt–TiO$_2$–Nb$_2$O$_5$ | Ketoprofen | UV LEDs | n.m. | 0.174 min$^{-1}$ | [102a] |
| 20 | Nb$_2$O$_5$ | Caffeic acid | White LED | 25 | ≈55% (180 min) | [127] |
| 21 | Pt–TiO$_2$–Nb$_2$O$_5$ | Diclofenac | UV LEDs | n.m. | 0.446 min$^{-1}$ | [102a] |
| 22 | Nb$_2$O$_5$ | Oxalic acid | 300 W Xe lamp | 25 | 40% (240 min) | [128] |
| 23 | Mesoporous Nb$_2$O$_5$ | Terephthalic acid | 400 W Hg lamp | 25 | 100% (60 min) | [129] |
| 24 | Nb$_2$O$_5$/C$_3$N$_4$ | Tetracycline hydrochloride | 250 W Xe lamp ($\lambda > 420$ nm) | 25 | 76% (150 min) | [116] |
| 25 | g-C$_3$N$_4$–mesoporous Nb$_2$O$_5$ | Tetracycline hydrochloride | 300 W Xe lamp ($\lambda > 420$ nm) | n.m. | 76% (60 min) | [99h] |
| 26 | Zn–Nb$_2$O$_5$ | Caffeic acid | 15 W UV light | r.t. | 80% (180 min) | [85j] |
| 27 | Fe$_2$O$_3$/Nb$_2$O$_5$ | Ethyl 4-hydroxy-benzoate | 300 W Xe lamp ($\lambda > 400$ nm) | n.m. | ≈55% (12 h) | [130] |
| 28 | NiO–Nb$_2$O$_5$ | Indigo carmine | 20 W UV light | n.m. | ≈90% (90 min) | [131] |
| 29 | Zr–Nb$_2$O$_5$ | Indigo carmine | 400 W halide lamp (350–700 nm) | 30 | 0.52 h$^{-1}$ | [77] |
| 30 | Nb$_2$O$_5$ | Indigo carmine | 125 W Hg lamp | n.m. | 100% (25 min) | [132] |
| 31 | TT-Nb$_2$O$_5$ particles | Indigo carmine | 400 W halide lamp (350–700 nm) | 30 | 0.29 h$^{-1}$ | [77] |
| 32 | TiO$_2$/Nb$_2$O$_5$ | Indigo carmine | 36 W UV lamp (200–400 nm) | n.m. | ≈87% (120 min) | [103a] |
| 33 | Nb$_2$O$_5$/cellulose acetate | Indigo carmine | 125 W Hg lamp | n.m. | ≈99% (120 min) | [133] |
| 34 | Nb$_2$O$_5$ hollow spheres | Indigo carmine | 100 W Hg lamp | n.m. | ≈90% (80 min) | [109a] |
| 35 | g-C$_3$N$_4$/Nb$_2$O$_5$ | Malachite green | 150 W white LED light | n.m. | 100% (90 min) | [109b] |
| 36 | Amorphous Nb$_2$O$_5$ particles | Malachite green | 400 W Hg lamp | 25 | 0.014 min$^{-1}$ | [65a] |
| 37 | Ag/TiO$_2$/Nb$_2$O$_5$ | Malachite green | Visible light | 25 | 100% (20 min) | [92b] |
| 38 | TT-Nb$_2$O$_5$ particles | Orange G | 400 W halide lamp (350–700 nm) | 30 | 0.13 h$^{-1}$ | [77] |
| 39 | Sr–Nb$_2$O$_5$ | Orange G | 400 W halide lamp (350–700 nm) | 30 | 0.20 h$^{-1}$ | [77] |
| 40 | TT-Nb$_2$O$_5$ particles | MB$^{c)}$ | 400 W halide lamp (350–700 nm) | 30 | 0.19 h$^{-1}$ | [77] |
| 41 | Sr–Nb$_2$O$_5$ | MB | 400 W halide lamp (350–700 nm) | 30 | 0.60 h$^{-1}$ | [77] |
| 42 | Nb$_2$O$_5$ | MB | 100 W Hg lamp | 25 | ≈90% (120 min) | [109c] |
| 43 | TT-Nb$_2$O$_5$ nanorods | MB | UV light | r.t. | 0.0733 min$^{-1}$ | [33a] |
| 44 | TT-Nb$_2$O$_5$ nanorods | MB | 500 W Hg lamp | r.t. | ≈93% (150 h) | [34c] |
| 45 | Mesoporous Nb$_2$O$_5$ | MB | 250 W Xe lamp | 30 | 0.014 min$^{-1}$ | [134] |
| 46 | TT-Nb$_2$O$_5$ spheres | MB | 500 W Hg lamp | r.t. | ≈73% (150 h) | [34c] |
| 47 | TT-Nb$_2$O$_5$ fibers | MB | 500 W Hg lamp | n.m. | 96% (50 min) | [68] |
| 48 | H-Nb$_2$O$_5$ particles | MB | 15 W UV light | 30 | 0.198 h$^{-1}$ | [135] |

(Continued)

**ADVANCED
SCIENCE NEWS**

www.advancedsciencenews.com

**ADVANCED
SCIENCE**
Open Access

www.advancedscience.com

**Table 1.** Continued.

| No. | Catalysts | Pollutants | Light sources | Reaction temperature [°C] | Degradation rate | Refs. |
|---|---|---|---|---|---|---|
| 49 | T-Nb$_2$O$_5$ particles | MB | UV lamp | r.t. | 60% (60 min) | [74] |
| 50 | Mixed phase Nb$_2$O$_5$ particles | MB | UV lamp | n.m. | 95% (120 min) | [136] |
| 51 | Nb$_2$O$_5$ nanofibers | MB | 300 W Xe lamp | n.m. | 45% (120 min) | [137] |
| 52 | Nb$_2$O$_5$ fibers | MB | 100 W Hg lamp | n.m. | 0.025 min$^{-1}$ | [138] |
| 53 | Nb$_2$O$_5$ | MB | 300 W Hg lamp | r.t. | 70% (480 min) | [139] |
| 54 | Nb$_2$O$_5$ nanoparticles | MB | 150 W Hg lamp | 25 | 90% (150 min) | [140] |
| 55 | Nb$_2$O$_5$ | MB | 450 W solar simulator | n.m. | 90% (20 min) | [141] |
| 56 | Nb$_2$O$_5$ | MB | 24 W lamps | 25 | 40% (80 min) | [142] |
| 57 | Nb$_2$O$_5$ | MB | UV light | n.m. | 40% (300 min) | [143] |
| 58 | N–Nb$_2$O$_5$ | MB | 500 W Xe lamp | 25 | 40% (240 min) | [87] |
| 59 | Mo–Nb$_2$O$_5$W–Nb$_2$O$_5$ | MB | UV light | 25 | n.m. | [85h] |
| 60 | Pd-xerogel/Nb$_2$O$_5$ | MB | Visible light | r.t. | 30% (300 min) | [85i] |
| 61 | Nb$_2$O$_5$/TiO$_2$ | MB | 400 W Xe lamp | n.m. | 0.072 min$^{-1}$ | [101a] |
| 62 | Nb$_2$O$_5$–TiO$_2$ | MB | UV light | r.t. | 100% (240 min) | [99a] |
| 63 | Nb$_2$O$_5$/TiO$_2$ | MB | 15 W fluorescent lamps (390–720 nm) | n.m. | 84% (150 min) | [111a] |
| 64 | Nb$_2$O$_5$/NaX zeolite | MB | 80 W Xe lamp | 25 | 60% (300 min) | [144] |
| 65 | Nb$_2$O$_5$/MCM-41 | MB | 15 W UV lamp | n.m. | 60% (60 min) | [145] |
| 66 | Nb$_2$O$_5$/Nb$_3$O$_7$F | MB | Xe lamp (380–780 nm) | r.t. | 100% (80 min) | [106] |
| 67 | α-Fe$_2$O$_3$/Nb$_2$O$_5$ | MB | 300 W simulated solar irradiation | n.m. | 80% (120 min) | [111b] |
| 68 | CdS@Nb$_2$O$_5$ | MB | 125 W Hg lamp | n.m. | 80% (180 min) | [97b] |
| 69 | Carbon xerogel–Nb$_2$O$_5$ | MB | Visible light | r.t. | 30% (300 min) | [146] |
| 70 | Carbon xerogel–Nb$_2$O$_5$ | MB | Visible light | 25 | 60% (300 min) | [147] |
| 71 | Nb$_2$O$_5$/tannin-formaldehyde xerogel | MB | 300 W UV lamp (200–280 nm) | 25 | 100% (90 min) | [148] |
| 72 | Carbon xerogel–Nb$_2$O$_5$ | MB | 300 W simulated solar | r.t. | 80% (300 min) | [149] |
| 73 | CeO$_2$/Nb$_2$O$_5$ | MB | UV light | n.m. | 98% (150 min) | [122] |
| 74 | g-C$_3$N$_4$/Nb$_2$O$_5$ | MB | UV light | 18 | 90% (210 min) | [99f] |
| 75 | TT-Nb$_2$O$_5$ spheres | MB | Xe lamp (λ > 380 nm) | r.t. | 90% (90 min) | [71a] |
| 76 | Nb$_2$O$_5$–graphene | MB | UV light | n.m. | 99% (5 min) | [150] |
| 77 | T-Nb$_2$O$_5$ nanowires | MB | 100 W mercury lamp | r.t. | 95% (150 min) | [37a] |
| 78 | Nb$_2$O$_5$–C$_{60}$ | MB | UV lamp | n.m. | 97% (5 min) | [102b] |
| 79 | Ag/Nb$_2$O$_5$ | MB | 500 W mercury lamp | n.m. | 0.0108 min$^{-1}$ | [151] |
| 80 | TiO$_2$/Nb$_2$O$_5$/r-GO | MB | 300 W Xe lamp | 24–28 | 97% (240 min) | [152] |
| 81 | MnO$_2$/Nb$_2$O$_5$/carbon clusters | MB | Visible light (λ > 460 nm) | n.m. | n.m. | [153] |
| 82 | N-TiO$_2$–Nb$_2$O$_5$ | MB | 13 W fluorescent lamp | n.m. | 66% (180 min) | [154] |
| 83 | Nb$_2$O$_5$ nanowires | MB | UV light | r.t. | 92% (120 min) | [155] |
| 84 | Nb$_2$O$_5$ nanoplates | MB | 100 W Hg lamp | r.t. | ≈92% (60 min) | [156] |
| 85 | Ag/TiO$_2$/Nb$_2$O$_5$ | MO[d)] | Visible light | 25 | 12% (120 min) | [92b] |
| 86 | r-GO/SnO$_2$/Nb$_2$O$_5$/TiO$_2$ | MO | 300 W Xe lamp (λ > 400 nm) | 30–35 | 95% (120 min) | [109f] |
| 87 | TiO$_2$/Nb$_2$O$_5$/r-GO | MO | 300 W Xe lamp | 30–35 | 93% (240 min) | [152] |
| 88 | T-Nb$_2$O$_5$ nanowires | MO | 100 W Hg lamp | r.t. | 70% (150 min) | [37a] |
| 89 | Nb$_2$O$_5$ nanofibers | MO | 300 W Hg lamp | r.t. | 62% (180 min) | [157] |
| 90 | Nb$_2$O$_5$ | MO | 400 W Hg lamp | r.t. | 78% (80 min) | [158] |
| 91 | Nb$_2$O$_5$ | MO | Sunlight | 25 | 95% (60 min) | [159] |
| 92 | Ag$_3$PO$_4$/Nb$_2$O$_5$ | MO | 600 W Xe lamp | n.m. | 100% (25 min) | [160] |
| 93 | Nb$_2$O$_5$@G nanofibers | MO | 400 W metal-halide lamp (λ > 380 nm) | n.m. | 0.547 h$^{-1}$ | [161] |
| 94 | Nb$_2$O$_5$/SrNb$_2$O$_6$ | MO | 300 W Hg lamp | n.m. | 95% (40 min) | [100b] |
| 95 | Nb$_2$O$_5$/SrNb$_2$O$_6$ | MO | 500 W Hg lamp | n.m. | ≈95% (28 min) | [162] |
| 96 | T-Nb$_2$O$_5$ particles | RhB[e)] | UV light | 25 | 61% (120 min) | [163] |

*(Continued)*

**Table 1.** Continued.

| No. | Catalysts | Pollutants | Light sources | Reaction temperature [°C] | Degradation rate | Refs. |
|---|---|---|---|---|---|---|
| 97 | TT-$Nb_2O_5$ particles | RhB | UV light | 18 | 0.00 757 $min^{-1}$ | [164] |
| 98 | TT-$Nb_2O_5$ particles | RhB | UV light | n.m. | 100% (60 min) | [165] |
| 99 | Amorphous $Nb_2O_5$ particles | RhB | 5 W white LED light | n.m. | 96% (70 min) | [166] |
| 100 | Flowerlike T-$Nb_2O_5$ | RhB | 300 W Hg lamp | r.t. | 100% (90 min) | [167] |
| 101 | T-$Nb_2O_5$ spheres | RhB | 300 W Xe lamp ($\lambda > 420$ nm) | n.m. | 0.2099 $min^{-1}$ | [112] |
| 102 | $Nb_2O_5$ | RhB | UV light | 25 | 78% (120 min) | [168] |
| 103 | $Nb_2O_5$ microflowers | RhB | 50 W Hg lamp | n.m. | 0.238 $min^{-1}$ | [169] |
| 104 | $Nb_2O_5$ | RhB | 8 W Hg lamp | r.t. | 0.0669 $min^{-1}$ | [170] |
| 105 | $Nb_2O_5$ nanoplates | RhB | 100 W Hg lamp | r.t. | ≈98% (60 min) | [156] |
| 106 | C-modified $Nb_2O_5$ | RhB | 500 W tungsten halogen lamp | n.m. | 100% (180 min) | [171] |
| 107 | C–$Nb_2O_5$ | RhB | Xe lamp | n.m. | 100% (30 min) | [82a] |
| 108 | N–$Nb_2O_5$ | RhB | 300 W Xe lamp ($\lambda > 400$ nm) | n.m. | 100% (15 min) | [88] |
| 109 | C, N-modified $Nb_2O_5$ | RhB | 300 W Xe lamp ($\lambda > 420$ nm) | 15 | 100% (40 min) | [172] |
| 110 | C, N-modified $Nb_2O_5$ | RhB | 300 W Xe lamp (420–720 nm) | n.m. | 0.13 572 $min^{-1}$ | [173] |
| 111 | N, S–$Nb_2O_5$ | RhB | UV light | n.m. | 92% (180 min) | [89] |
| 112 | N–$HNb_3O_8$ | RhB | 300 W Xe lamp ($\lambda > 420$ nm) | n.m. | 98% (50 min) | [174] |
| 113 | C–$Nb_2O_5$ | RhB | 300 W Xe lamp ($\lambda > 420$ nm) | 25 | ≈90% (30 min) | [175] |
| 114 | N–$HNb_3O_8$ | RhB | 300 W Xe lamp ($\lambda > 420$ nm) | n.m. | 98% (50 min) | [176] |
| 115 | Au@void@$Nb_2O_5$ | RhB | 300 W Xe lamp ($\lambda > 420$ nm) | 15 | 100% (140 min) | [92a] |
| 116 | $Nb_2O_5$/Pd@SBA-15 | RhB | UV light | r.t. | 97% (210 min) | [177] |
| 117 | $Nb_2O_5$/FTO | RhB | 300 W Hg lamp | n.m. | 0.01 212 $min^{-1}$ | [178] |
| 118 | BiOCl/$Nb_2O_5$/$Bi_4NbO_8Cl$ | RhB | 300 W Hg lamp | n.m. | 99% (40 min) | [179] |
| 119 | $Nb_2O_5$–g-$C_3N_4$/graphene aerogel | RhB | 300 W Xe lamp ($\lambda > 420$ nm) | n.m. | 95% (100 min) | [180] |
| 120 | $BiNb_5O_{14}$/$Nb_2O_5$ | RhB | 500 W Xe lamp ($\lambda > 420$ nm) | n.m. | 61% (60 min) | [181] |
| 121 | $Nb_2O_5$–$WO_3$ | RhB | 125 W Hg lamp | n.m. | ≈70% (100 min) | [182] |
| 122 | TT-$Nb_2O_5$ particles | RhB | UV light | 18 | 0.00 323 $min^{-1}$ | [109e] |
| 123 | g-$C_3N_4$/$Nb_2O_5$ | RhB | 15 W fluorescent lamps | 18 | 0.0202 $min^{-1}$ | [13] |
| 124 | T-$Nb_2O_5$ nanowires | RhB | 100 W Hg lamp | r.t. | 95% (150 min) | [37a] |
| 125 | C–$Nb_2O_5$ | RhB | 300 W Xe lamp ($\lambda > 420$ nm) | n.m. | 100% (30 min) | [82b] |
| 126 | TT-$Nb_2O_5$ nanowires | RhB | 500 W Xe lamp ($\lambda > 420$ nm) | n.m. | 0.047 $min^{-1}$ | [183] |
| 127 | g-$C_3N_4$–mesoporous $Nb_2O_5$ | RhB | 300 W Xe lamp ($\lambda > 420$ nm) | n.m. | 98% (180 min) | [99h] |
| 128 | Zn–$Nb_2O_5$ | RhB | 15 W UV light | r.t. | 90% (180 min) | [85j] |
| 129 | Zn–C/$Nb_2O_5$ | RhB | Visible light | n.m. | 100% (80 min) | [184] |
| 130 | $Cd_xZn_yS$/$Nb_2O_5$ | Violet | 100 W fluorescent lamps | n.m. | 0.054 $min^{-1}$ | [104b] |
| 131 | r-GO/$SnO_2$/$Nb_2O_5$/$TiO_2$ | Violet | 300 W Xe lamp ($\lambda > 400$ nm) | 30–35 | 98% (120 min) | [109f] |
| 132 | TT-$Nb_2O_5$ particles | Atrazine | UV light | 18 | 0.0124 $min^{-1}$ | [164] |
| 133 | TT-$Nb_2O_5$ particles | Atrazine | UV light | 18 | 0.03 $min^{-1}$ | [109e] |
| 134 | $Nb_2O_5$ | Basic red-2 | 400 W Hg lamp | 25 | 94% (120 min) | [185] |
| 135 | Mesoporous TT-$Nb_2O_5$ particles | Methylviologen | 125 W Hg lamp | 25 | 0.041 $min^{-1}$ | [186] |
| 136 | $Fe_2O_3$/$Nb_2O_5$ | Triclosan | 125 W Hg lamp | 25 | 0.069 $min^{-1}$ | [187] |
| 137 | $Nb_2O_5$/bentonite clay | Blue 19 | 125 W Hg lamp | 25 | 98% (120 min) | [188] |
| 138 | $Nb_2O_5$/activated charcoal | Blue 5G | 250 W Hg lamp | 28 | ≈94 (300 min) | [189] |
| 139 | ZnO/$Nb_2O_5$ | Bromophenol blue | 400 W Hg lamp | 25 | 0.030 $min^{-1}$ | [104a] |
| 140 | $Nb_2O_5$/ZnAl-LDH | Congo red | 300 W Xe lamp ($\lambda > 420$ nm) | n.m. | ≈85% (390 min) | [190] |
| 141 | $Nb_2O_5$/$Bi_2WO_6$ | Dibenzo-thiophene | 5 W LED lamps | r.t. | 99% (120 min) | [191] |
| 142 | $Nb_2O_5$ | Reactive blue 59 | 400 W Hg lamp | n.m. | 89% (150 min) | [192] |
| 143 | TT-$Nb_2O_5$ spheres | Rose bengal | Xe lamp ($\lambda > 380$ nm) | r.t. | 60% (180 min) | [71a] |
| 144 | g-$C_3N_4$/$Nb_2O_5$ | Amiloride | 15 W fluorescent lamps | 18 | 0.0137 $min^{-1}$ | [13] |

*(Continued)*

**ADVANCED
SCIENCE NEWS**

www.advancedsciencenews.com

**ADVANCED
SCIENCE**

Open Access

www.advancedscience.com

**Table 1.** Continued.

| No. | Catalysts | Pollutants | Light sources | Reaction temperature [°C] | Degradation rate | Refs. |
|---|---|---|---|---|---|---|
| 145 | HNb$_3$O$_8$ nanosheets | Bromocresol green | Hg lamp | 20–25 | ≈90% (45 min) | [50e] |
| 146 | Fe$_2$O$_3$/Nb$_2$O$_5$ | Paper wastewater | 205 W Hg lamp | r.t. | 0.061 h$^{-1}$ | [113a] |
| 147 | Ag$_2$O/Nb$_2$O$_5$ | Paper wastewater | 205 W Hg lamp | r.t. | 0.094 h$^{-1}$ | [113a] |
| 148 | Nb$_2$O$_5$ | Textile wastewater | 250 W Hg lamp | 25 | ≈0.60 min$^{-1}$ | [113b] |
| 149 | Carbon black–Nb$_2$O$_5$ | Textile wastewater | 250 W Hg lamp | n.m. | ≈41% (300 min) | [113c] |
| 150 | Ag/Nb$_2$O$_5$ | Textile dyes | UV light bulb | n.m. | ≈96% (24 h) | [193] |
| 151 | Nb$_2$O$_5$/NaX | Textile effluents | 250 W Hg lamp | 28 | 0.0033 min$^{-1}$ | [194] |
| 152 | Nb$_2$O$_5$/ZnO | Palm oil mill effluent | 15 W UV lamp | n.m. | 92% (240 min) | [195] |
| 153 | Nb$_2$O$_5$/ZnO | Palm oil mill efuent | 15 W UV lamp | n.m. | 92% (240 min) | [196] |
| 154 | Nb$_2$O$_5$ | Petrol station wastewater | 250 W Hg lamp | n.m. | ≈35% (300 min) | [197] |
| 155 | Nb$_2$O$_5$–TiO$_2$ | Vinasse | Solar radiation | n.m. | ≈55% (24 h) | [100a] |
| 156 | Nb$_2$O$_5$/TiO$_2$ | Cr(VI) | 20 W UV lamp | n.m. | ≈90% (180 min) | [99c] |
| 157 | TT-Nb$_2$O$_5$ nanowires/carbon fiber | Cr(VI) | 500 W UV light | n.m. | ≈99% (60 min) | [198] |
| 158 | TT-Nb$_2$O$_5$ nanorods/diatomite | Cr(VI) | 500 W Hg lamp | r.t. | 90% (60 min) | [199] |
| 159 | Porous TT-Nb$_2$O$_5$ | Cr(VI) | 18 W UV light | n.m. | 60% (120 min) | [63b] |
| 160 | Nb$_2$O$_5$ | Cr(VI) | 250 W Hg lamp | n.m. | ≈90% (120 min) | [200] |
| 161 | N-modified Nb$_2$O$_5$ | Cr(VI) | Visible light ($\lambda > 420$ nm) | n.m. | ≈80% (240 min) | [117] |
| 162 | CuO/Nb$_2$O$_5$ | Cr(VI) | 15 W UV lamps | 18 | 23.10 min$^{-1}$ | [201] |
| 163 | Nb$_2$O$_5$@MIL-125 | Cr(VI) | 990 W Xe lamp | 25 | ≈99% (60 min) | [202] |
| 164 | TT-Nb$_2$O$_5$ particles | *Escherichia coli* | Black light lamp | n.m. | 0.034 min$^{-1}$ | [203] |
| 165 | Sr–Nb$_2$O$_5$ | *Escherichia coli* | 400 W halide lamp (350–700 nm) | 30 | 0.12 min$^{-1}$ | [77] |
| 166 | Sr–Nb$_2$O$_5$ | *Staphylococcus aureus* | 400 W halide lamp (350–700 nm) | 30 | 0.069 min$^{-1}$ | [77] |

a) Not mentioned  b) Room temperature  c) Methylene blue  d) Methyl orange  e) Rhodamine B.

comparison of activity. These phenomena can be ascribed to the complex reaction mechanism and the difficulty in the product analysis. Further studies in this area are still necessary.

Pure Nb$_2$O$_5$, N–Nb$_2$O$_5$, and composited Nb$_2$O$_5$ photocatalysts were also applied in the removal of toxic Cr(VI) species (Table 1, Nos. 156–163).[77,99c,117] Unlike the degradation of organic pollutants, the Cr(VI) species are reduced by the photogenerated electrons (Figure 7, path C). Besides, the utilization of Nb$_2$O$_5$-based photocatalysts was also reported in the inactivation of bacteria (Table 1, Nos. 164–166). The *Staphylococcus aureus* and *Escherichia coli* were inactivated by ●O$_2^-$ species that were generated from the reaction between O$_2$ and excited electrons on the Nb$_2$O$_5$ surface (Figure 7, path A).[77] Considering the nontoxic demand for drugs, these results imply the potential application of Nb$_2$O$_5$-based photocatalysts in the medical field.

### 4.2. Photocatalytic H$_2$ and O$_2$ Evolution

Photocatalytic hydrogen evolution is the potential process to produce H$_2$ as a clean energy carrier.[5b,204] Generally, the excited electrons in semiconductor photocatalysts are utilized for the reduction of H$^+$ ions or H$_2$O to H$_2$.[5b] However, the reaction rate over Nb$_2$O$_5$ is limited by several factors, including i) the high recombination efficiency of charge carriers, ii) the low reduction rate of catalytic protons to H$_2$, iii) the insufficient absorption capacity of visible light, and so on. Thus, some strategies have been devel-

oped to enhance the photocatalytic performance.[5b] For instance, sacrificial agents, like triethanolamine (TEOA), methanol, lactic acid, Na$_2$S, and Na$_2$SO$_3$, were introduced into the reaction mixture to consume the holes on Nb$_2$O$_5$-based photocatalysts while the remaining electrons were still utilized for the production of H$_2$ (**Table 2**, Nos. 1–32).[103b,205] Modified Nb$_2$O$_5$ with platinum as a cocatalyst was introduced to promote the reduction of protons to H$_2$ (Table 2, Nos. 1–5). Similarly, Nb$_2$O$_5$ can be modified with Au and sulfide to enhance the hydrogen evolution rate (Table 2, Nos. 24, 28–29, 31). Meanwhile, the obtained catalyst is active under visible light irradiation (Table 2, No. 4).

Furthermore, the Nb$_2$O$_5$ and Pt/Nb$_2$O$_5$ were applied in the oxidation of water to O$_2$ (Table 2, Nos. 33–34). In this process, AgNO$_3$ acted as the sacrificial agent, which was reduced by the photogenerated electrons on Nb$_2$O$_5$-based photocatalysts. Especially, the apparent quantum yield (AQY) was mentioned in these processes (Table 2, Nos. 2–4), which is defined by the number of the reacted electrons to the number of incident photons.[206] The AQY can be a benchmark for comparison of efficiency in different photocatalytic systems. Recently, the AQY in the photocatalytic water splitting to H$_2$ and O$_2$ was up to ≈96% on Al–SrTiO$_3$ under 360 nm light irradiation.[207] This result is much higher than that reported on Nb$_2$O$_5$-based catalysts (Table 2, Nos. 2–4). Hence, the challenge and opportunity are still present in further improving the activity of Nb$_2$O$_5$-based photocatalysts.

**ADVANCED
SCIENCE NEWS**

www.advancedsciencenews.com

**ADVANCED
SCIENCE**

Open Access

www.advancedscience.com

**Table 2.** Recent advances in the photocatalytic $H_2$ and $O_2$ evolution over $Nb_2O_5$-based photocatalysts.

| No. | Catalysts | Products | Sacrificial agents | Light sources | Reaction temperature [°C] | Reaction rate [μmol g$^{-1}$ h$^{-1}$] | AQY[a] [%] | Refs. |
|---|---|---|---|---|---|---|---|---|
| 1 | Pt/H-$Nb_2O_5$ nanorods | $H_2$ | Methanol | 500 W Hg lamp | n.m.[b] | ≈1820 | n.m. | [205b] |
| 2 | Pt/TT-$Nb_2O_5$ nanowires | $H_2$ | Methanol | 300 W Xe lamp | 25 | 680 | 4.7 | [40a] |
| 3 | Pt/TT-$Nb_2O_5$ nanowires | $H_2$ | Methanol | 300 W Xe lamp ($λ > 300$ nm) | n.m. | ≈780 | 4.6 | [40b] |
| 4 | Pt/N-$HNb_3O_8$ nanosheets | $H_2$ | Methanol | 300 W Xe lamp ($λ > 420$ nm) | n.m. | ≈1200 | 1.69 | [50f] |
| 5 | Pt/$Nb_2O_5$ | $H_2$ | Methanol | 400 W Hg lamp | 20 | 12 350 | n.m. | [20] |
| 6 | CuO/$Nb_2O_{5-x}$ | $H_2$ | Methanol | 300 W white light | 50 | 1405 | n.m. | [69] |
| 7 | $Nb_2O_5$ nanoparticles | $H_2$ | Methanol | 300 W Hg lamp | 25–27 | 191 | n.m. | [208] |
| 8 | Pt/C–$Nb_2O_5$ | $H_2$ | Methanol | 300 W Xe lamp ($λ > 420$ nm) | n.m. | ≈39 | n.m. | [82b] |
| 9 | Pt/N–$Nb_2O_5$ | $H_2$ | Methanol | 150 W Xe lamp ($λ > 400$ nm) | 25 | 154 | n.m. | [19] |
| 10 | Pt/N–$Nb_2O_5$ | $H_2$ | Methanol | 400 W Hg lamp | r.t.[c] | 3010 | n.m. | [84] |
| 11 | N–$Nb_2O_5$/r-GO | $H_2$ | Methanol | Sunlight | n.m. | 5370 | 4.5 | [83a] |
| 12 | Carbonaceous $Nb_2O_5$ | $H_2$ | Methanol | 500 W Xe lamp | n.m. | 2 | n.m. | [209] |
| 13 | Pt/$Nb_2O_5$ | $H_2$ | Methanol | 400 W halide lamp | 43 | 4647 | n.m. | [95b] |
| 14 | Pt/$Nb_2O_5$ | $H_2$ | Methanol | 150 W solar simulator | r.t. | ≈25 | 1.06 | [210] |
| 15 | Pt/$Nb_2O_5$ | $H_2$ | Methanol | 165 W Hg lamp | 10 | 9790 | n.m. | [211] |
| 16 | NiO QDs/$Nb_2O_5$ | $H_2$ | Methanol | 300 W Xe lamp | n.m. | 124 | n.m. | [212] |
| 17 | Pt/$Nb_2O_5$/$TiO_2$ | $H_2$ | Methanol | 200 W Xe lamp (320–780 nm) | n.m. | 1800 | n.m. | [213] |
| 18 | Er–$Y_3Al_5O_{12}$@ $Nb_2O_5$/Pt/$In_2O_3$ | $H_2$ | Methanol | 300 W Xe lamp (420–800 nm) | 25 | ≈100 | n.m. | [214] |
| 19 | $Nb_2O_5$/$MoS_2$/graphene | $H_2$ | Methanol | Visible light | r.t. | 136 800 | n.m. | [215] |
| 20 | $Nb_2O_5$/C/$Nb_2C$ | $H_2$ | Methanol | 200 W Hg lamp | 25 | ≈8 | 0.11 | [97d] |
| 21 | Pt/$Nb_2O_5$–r-GO | $H_2$ | Methanol | 150 W Xe lamp ($λ > 400$ nm) | 25 | ≈882 | 13 | [216] |
| 22 | Pt/$Nb_2O_5$–N-doped graphene | $H_2$ | Methanol | 150 W Xe lamp ($λ > 400$ nm) | r.t. | ≈24 | n.m. | [97e] |
| 23 | Pt/$Nb_2O_5$ | $H_2$ | Methanol | 400 W Hg lamp | n.m. | 1120 | >6 | [70] |
| 24 | Au/$Nb_2O_5$ | $H_2$ | Methanol | 500 W Xe lamp | n.m. | ≈11 | n.m. | [166] |
| 25 | Pt/C-modified $Nb_2O_5$ | $H_2$ | Methanol | 300 W Xe lamp ($λ > 420$ nm) | n.m. | 7 | n.m. | [171] |
| 26 | Pt/g-$C_3N_4$/$Nb_2O_5$ | $H_2$ | TEOA[d] | 300 W Xe lamp ($λ > 400$ nm) | <6 | 1710 | n.m. | [99g] |
| 27 | Pt/g-$C_3N_4$/$Nb_2O_5$ | $H_2$ | TEOA | 1000 W Xe lamp | n.m. | 110 000 | n.m. | [205d] |
| 28 | Pt/$Nb_2O_5$/$ZnIn_2S_4$ | $H_2$ | TEOA | 300 W Xe lamp | 5 | 6026 | 3.75 | [217] |
| 29 | $Nb_2O_5$–$SnS_2$–CdS | $H_2$ | Lactic acid | 300 W Xe lamp | r.t. | ≈3600 | 0.65 | [205a] |
| 30 | Pt/$Nb_2O_5$ | $H_2$ | $Na_2SO_3$ | 300 W Xe lamp ($λ > 420$ nm) | n.m. | 130 | n.m. | [205c] |
| 31 | CdS/$Nb_2O_5$/N-doped graphene | $H_2$ | $Na_2S$ and $Na_2SO_3$ | 150 W Xe lamp ($λ > 400$ nm) | 25 | ≈96 | 1.5 | [103b] |
| 32 | TT-$Nb_2O_5$ nanowires | $H_2$ | $Na_2S$ and $Na_2SO_3$ | 500 W Xe lamp ($λ > 420$nm) | n.m. | ≈244 | n.m. | [183] |
| 33 | Pt/TT-$Nb_2O_5$ nanowires | $O_2$ | $AgNO_3$ | 300 W Xe lamp | 25 | 70 | n.m. | [40a] |
| 34 | TT-$Nb_2O_5$ nanowires | $O_2$ | $AgNO_3$ | 300 W Xe lamp ($λ > 300$ nm) | n.m. | ≈620 | n.m. | [40b] |

[a] Apparent quantum yield [b] Not mentioned [c] Room temperature [d] Triethanolamine.

## 4.3. Photoreduction of $CO_2$

$CO_2$ as a carbonaceous resource can be applied in the production of chemicals and fuels.[218] For instance, $CO_2$ can be reduced to one-carbon ($C_1$) molecules, like CO, HCOOH, HCHO, $CH_3OH$, and $CH_4$, and $C_{2+}$ products.[218] There are two typical reaction modes for photocatalytic reduction of $CO_2$: solid–liquid interface reaction mode (mode I) and solid–vapor interface reaction mode (mode II).[219] In the first mode, the photocatalysts were introduced into an aqueous solution. Dissolved $CO_2$ in water can be reduced on the solid–liquid interface. For another one, $CO_2$ molecules were directly reduced on the solid-photocatalysts surface. Especially, two modes were both reported with the uti-

lization of $Nb_2O_5$-based photocatalysts.[9b,220] The CO, HCOOH, $CH_3OH$, $CH_4$, and $CH_3COOH$ were observed in these reduction process (**Table 3**).[9b,220] Because the dissolved $CO_2$ in water is limited in mode I that was widely reported, sacrificial agents, such as triethylamine, were added to improve the solubility of $CO_2$ in water and consumed the excited holes. Besides, the photoreduction of $CO_2$ can be occurred on amorphous $Nb_2O_5$ without any additives (Table 3, No. 3). Some possible reaction pathways were proposed as following Equations (1)–(8)[9a,219]

$$CO_2 + 2H^+ + 2e^- \rightarrow HCOOH \tag{1}$$

$$CO_2 + 2H^+ + 2e^- \rightarrow CO + H_2O \tag{2}$$

**Table 3.** Recent advances in the photocatalytic reduction of $CO_2$ over $Nb_2O_5$-based photocatalysts.

| No. | Catalysts | Substrates | Main product | Light sources | Reaction temperature [°C] | Reaction rate [μmol g$^{-1}$ h$^{-1}$] | Refs. |
|---|---|---|---|---|---|---|---|
| 1 | $In_2O_{3-x}(OH)_y/Nb_2O_5$ nanorods | $CO_2$ and $H_2$ | CO | 300 W Xe lamp | 60 | 1400 | [220a] |
| 2 | $HNb_3O_8$ nanobelts | $CO_2$ and $H_2O$ | $CH_4$ | 350 W Xe lamp | 45 | 3.58 | [220b] |
| 3 | Amorphous $Nb_2O_5$ | $CO_2$ and $H_2O$ | $CH_3COOH$ | UV light | n.m.[a] | ≈1.35 | [9b] |
| 4 | $SiO_2–HNb_3O_8$ | $CO_2$ and $H_2O$ | $CH_4$ | 350 W Xe lamp | 60 | 2.90 | [220c] |

[a] Not mentioned.

$$CO_2 + 4H^+ + 4e^- \rightarrow HCHO + H_2O \tag{3}$$

$$CO_2 + 6H^+ + 6e^- \rightarrow CH_3OH + H_2O \tag{4}$$

$$CO_2 + 8H^+ + 8e^- \rightarrow CH_4 + 2H_2O \tag{5}$$

$$CO_2 + H^+ + e^- \rightarrow \bullet COOH \tag{6}$$

$$2 \bullet COOH \rightarrow HCOOCOOH \tag{7}$$

$$HCOOCOOH + H^+ + e^- \rightarrow CH_3CHOOH \tag{8}$$
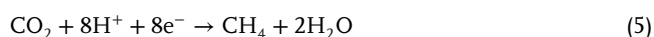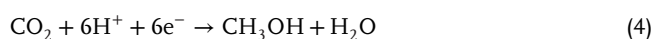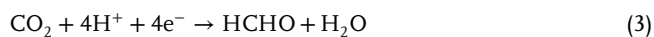
It is very important to underline some critical, analytical, and mechanistic aspects in the photocatalytic conversion of $CO_2$. Over the past decade, it is known that carbon residues can be involved in photocatalytic water activation and $CO_2$ reduction.[221] This is particularly relevant for the correct evaluation of the rates of artificial photosynthesis using photocatalysts synthesized with carbon-containing precursors. For this reason, it has become more and more relevant to the use of $^{13}CO_2$ to prove the mechanism of $CO_2$ reduction. In fact, the reaction products, often in trace levels, can derive also from light-induced desorption or reaction of carbonaceous impurities or residues from the synthesis in organic media that are not fully removed even by calcination. For instance, the $CH_4$ can be observed from the catalysts under light irradiation without $CO_2$.[220c] After eliminating the effects of carbon residues, the experimental results are conducive to reveal the process of photocatalytic reduction of $CO_2$. The photocatalytic efficiency can be evaluated by the AQY, which was not mentioned in these processes (Table 3).[9b,220] Besides, the selectivity of products is also important for catalytic performance. The $C_1$ products from $CO_2$ are important chemical intermediates and fuels.[218] High selectivity (>99%) of CO and $CH_4$ has been obtained, respectively (Table 3, Nos. 1–2). Although other acid products were observed in pure $Nb_2O_5$,[9d] the selectivity of HCOOH (35%) was competitive with that of $CH_3COOH$ (42%; Table 3, No.3). The formation of $CH_3COOH$ involved the C–C coupling reaction of •COOH radicals (Equations (6)–(8)).[9a] Unfortunately, the uncontrollable activity of •COOH radicals leads to the simultaneous generation of $CH_3COOH$ and HCOOH.[115] Besides, syngas that is vital in Fischer–Tropsch synthesis can be directly obtained from the reduction of $CO_2$ and $H_2$ evolution in photocatalysis.[222] To date, such processes are yet to be recognized over $Nb_2O_5$-based photocatalysts.

### 4.4. Selective Transformation of Organic Molecules

Amines, aldehydes, and ketones are important organic intermediates for medicines and polymers.[223] The VB maximum of $Nb_2O_5$ is up to ≈+2.50 V versus NHE (normal hydrogen electrode), implying its potential application in the oxidation and succedent transformation of organic molecules.[9a] The amines, alcohols, propene, cyclohexane, toluene, and ethylbenzene were selective oxidation to corresponding imines, aliphatic aldehydes, ketones, benzaldehyde, and acetophenone (**Table 4**). Similar to the photocatalytic reduction of $CO_2$ (Section 4.3), there were also two typical reaction modes in the selective transformation of organic molecules. In the first mode, $O_2$, solid photocatalysts, pure organic liquid, or the substrate dissolved in the solvent, like benzene and acetonitrile, were present in the system (Table 4, Nos. 1–16). For another one, the mixture of $O_2$, substrate, and solid photocatalysts were introduced into the reactor (Table 4, No. 17). The reaction rate of benzylamine observed on $Nb_2O_5$ was higher than that of $TiO_2$.[9c] Meanwhile, the selectivity of N-benzylidene benzylamine on $Nb_2O_5$ is up to 98%.[9c] Besides, the selectivity of partial oxidation products was up to 97% after the deposition of $Nb_2O_5$ on the $TiO_2$ surface under UV light irradiation.[97a] This may be attributed to that the amounts of photogenerated $O_3^-$ species over the catalyst drastically decreased, which were estimated by electron spin resonance spectroscopy.[97a] Interestingly, primary alcohols oxidized to aldehydes without the generation of acid on $Nb_2O_5$ under visible light irradiation.[224] A detailed relationship between product selectivity and structure of $Nb_2O_5$-based photocatalysts is summarized in the next section.

In addition, $Pd/HNb_3O_8$ nanosheets were efficient in the reduction of aryl nitro-compounds to aniline (Table 4, No. 18).[50c] Moreover, $Nb_2O_5$ catalysts were also applied in the photocatalytic coupling reaction. Xie's group demonstrated that the polyethylene was completely photodegraded on $Nb_2O_5$ nanosheets while generated $CO_2$ was further reduced to $CH_3COOH$ (Table 4, No. 19).[9a] Possible reaction mechanism was provided, in which $CO_2$ was reduced to •COOH radicals, HCOOCOOH, and $CH_3COOH$ (Section 4.3, Equations (6)–(8)).[9a] The transformation of waste plastics to chemicals and fuel can be realized by this process. Although the yield of $CH_3COOH$ is limited, further designs in photocatalysts are possible to enhance its activity. In addition, the acid sites on $Nb_2O_5$ play an important role in the coupling reaction. For instance, dimethoxymethane molecules were generated in the photooxidation methanol, indicating the coupling formaldehyde and methanol catalyzed by the BAS of $Au/Nb_2O_5$ (Table 4, No.

**ADVANCED**
**SCIENCE NEWS**
www.advancedsciencenews.com

**ADVANCED**
**SCIENCE**
Open Access
www.advancedscience.com

**Table 4.** Recent advances in the selective photooxidation of organic molecules over $Nb_2O_5$-based photocatalysts.

| No. | Catalysts | Substrates | Main products | Light sources | Reaction temperature [°C] | Reaction rate [$\mu$mol g$^{-1}$ h$^{-1}$][a] | AQY [%] | Refs. |
|---|---|---|---|---|---|---|---|---|
| 1 | $HNb_3O_8$ nanosheets | Amines | Imines | 300 W Xe lamp ($\lambda > 420$ nm) | 25 | ≈1979 | 6.57 | [12c] |
| 2 | $Nb_2O_5$ | Amines | Imines | 500 W Hg lamp | r.t.[b] | 1298 | ≈14 | [9c] |
| 3 | $Nb_2O_5$@NiFe-MMO | Benzyl-amine | Imine | 300 W Xe lamp | 30 | ≈18281 | n.m.[c] | [226] |
| 4 | $Nb_2O_5$/ZnMgAl-LDH | Anilines | Azoxy-benzenes | 50 W violet light LED | r.t. | ≈1979 | n.m. | [227] |
| 5 | $Nb_2O_5$ | 1-pentanol | Pentanal | 500 W Hg lamp | 50 | ≈1.28 | n.m. | [228] |
| 6 | $HNb_3O_8$ nanosheets | Benzylic alcohols | Benz-aldehyde | 300 W Xe lamp ($\lambda > 400$ nm) | 25 | ≈1969 | n.m. | [229] |
| 7 | $Nb_2O_5$ | Alcohols | Aldehydes and ketones | 500 W Hg lamp ($\lambda > 390$ nm) | 50 | ≈8.97 | ≈5.2 | [230] |
| 8 | $Nb_2O_5$ | Alcohols | Aldehydes and ketones | 500 W Hg lamp ($\lambda > 390$ nm) | r.t. | ≈619 | n.m. | [224] |
| 9 | $Nb_2O_5$ | HMF | DFF | 300 W Xe lamp | 30 | ≈333 | n.m. | [9e] |
| 10 | $Nb_2O_5$/$TiO_2$ | 1-pentanol | Pentanal | 500 W Hg lamp | r.t. | ≈8660 | n.m. | [97a] |
| 11 | $Nb_2O_5$/$TiO_2$ | Alcohols | Aldehydes and ketones | 500 W Hg lamp | r.t. | ≈48748 | n.m. | [231] |
| 12 | $Nb_2O_5$/$TiO_2$ | Aryl alcohols | Aldehydes and ketones | 200 W Xe lamp | n.m. | 17 600 | n.m. | [213] |
| 13 | $Nb_2O_5$/$SiO_2$ | Ethanol | Acet-aldehyde | 500 W Hg lamp ($\lambda > 320$ nm) | 37 | ≈107 | n.m. | [232] |
| 14 | $Nb_2O_5$ | CH[d] and EB[e] | Aldehydes and ketones | 500 W Hg lamp ($\lambda > 390$ nm) | r.t. | ≈120 | n.m. | [9d] |
| 15 | $Nb_2O_5$ | Toluene | Benz-aldehyde | 200 W Hg-Xe lamp ($\lambda > 390$ nm) | 20 | ≈80 | ≈11 | [18] |
| 16 | N–$Nb_2O_5$ | Toluene | Benz-aldehyde | 6 W LED | 40 | ≈28 | n.m. | [12b] |
| 17 | $Nb_2O_5$/$SiO_2$ | Propene | Aldehydes | 500 W Xe lamp ($\lambda > 290$ nm) | r.t. | ≈13 | n.m. | [233] |
| 18 | Pd/$HNb_3O_8$ nanosheets | Aryl nitro-compound | Aniline | 300 W Xe lamp ($\lambda > 320$ nm) | 25 | ≈2168 | n.m. | [50c] |
| 19 | $Nb_2O_5$ nanosheet | Plastics | $CH_3COOH$ | 300 W Xe lamp | 25 | ≈0.79 | n.m. | [9a] |
| 20 | Au/$Nb_2O_5$ | Methanol | DMM[f] | UV light | 25 | ≈2.64 | n.m. | [225] |
| 21 | $Nb_2O_5$/$ZnIn_2S_4$ | HMF[g] and $H_2O$ | DFF[h] and $H_2$ | Simulated solar light | 30 | ≈429 | n.m. | [217] |

[a] Productivity of the main product [b] Room temperature [c] Not mentioned [d] Cyclohexane [e] Ethylbenzene [f] Dimethoxymethane [g] 5-Hydroxymethylfurfural [h] 2,5-Diformylfuran.

20).[225] The other example reported by Lei's group demonstrated that 2,5-diformylfuran (DFF) and $H_2$ are produced from 5-hydroxymethylfurfural (HMF) and $H_2O$ on $Nb_2O_5$/$ZnIn_2S_4$, in which HMF acted as a sacrificial agent to consume the holes to improve the evolution of $H_2$ with the formation of DFF (Table 4, No. 21).[217] This strategy is available to improve the efficiency of photogenerated holes and electrons simultaneously.[7a]

# 5. The Structure–Activity Relationship

## 5.1. The Role of Size and Crystalline Phases

Previously, $Nb_2O_5$-based catalysts with high SSA can be efficient photocatalysts (**Figure 8**a–c).[70] In the degradation process of trichloroethylene, T-$Nb_2O_5$ nanotubes showed higher activity than that of layered $K_4Nb_6O_{17}$, which were ascribed to their higher crystallinity and specific surface area.[23c] After that, Zhang's group reported that H-$Nb_2O_5$ nanorods exhibited higher photocurrent density than that of commercial counterpart, due to the positive effect of high SSA on the separation of photogenerated carriers.[205b] Besides, the thickness of $Nb_2O_5$-based catalysts may play an important role in photocatalysis. Tsang's group reported that a higher photocatalytic $H_2$ evolution rate was observed with smaller numbers of the layer on $Nb_2O_5$-based nanosheets.[12c,43] In Yu's results, the photocatalytic $H_2$ evolution rate was enhanced with a decrease in the wall thickness of porous

$Nb_2O_5$.[20] These results imply a positive role of the thin-walled structure of $Nb_2O_5$ in the separation of charge carriers.

Although the crystal faces of $Nb_2O_5$, like (010), were revealed by the high-resolution transmission electron microscopy (HRTEM), the role of these structures is rarely reported in photocatalysis.[33a,234] Previously, Kudo's group afforded a possible explanation.[40b] In the photocatalytic $H_2$ evolution, higher activity of TT-$Nb_2O_5$ nanowires was observed than that of bulk counterpart in their results.[40b] Meanwhile, the Pt particles were selectively distributed on the short-axis plane of the TT-$Nb_2O_5$ nanowires in the photodeposition process. These results suggested that the photogenerated electrons moved along the nanowire growth direction while holes migrated to the nanowire sidewall.[40b] Although some Pt particles were also observed on other facets, Kudo's group described the mobility difference of charge carriers in the crystal growth direction. After that, the driving force can be ascribed to the formation of a built-in electric field between different facets, which is instructive to the separation of e$^-$ and h$^+$.[235] In addition, Tsang's group reported that {001} facet on $Nb_2O_5$ nanorods was active for photodegradation of methylene blue.[33a] This can be attributed to the strong Lewis acidity of $Nb_2O_5$ nanorods, which is summarized in Section 5.3.[33a]

Previously, TT-$Nb_2O_5$ exhibited a higher SSA and reactivity than those of T-$Nb_2O_5$ and H-$Nb_2O_5$.[9e,70,135] Whereas, some research groups found that T-$Nb_2O_5$ and H-$Nb_2O_5$ showed higher activity than that of TT-$Nb_2O_5$ in photodegradation of methylene

**ADVANCED
SCIENCE NEWS**

www.advancedsciencenews.com

**ADVANCED
SCIENCE**
Open Access

www.advancedscience.com
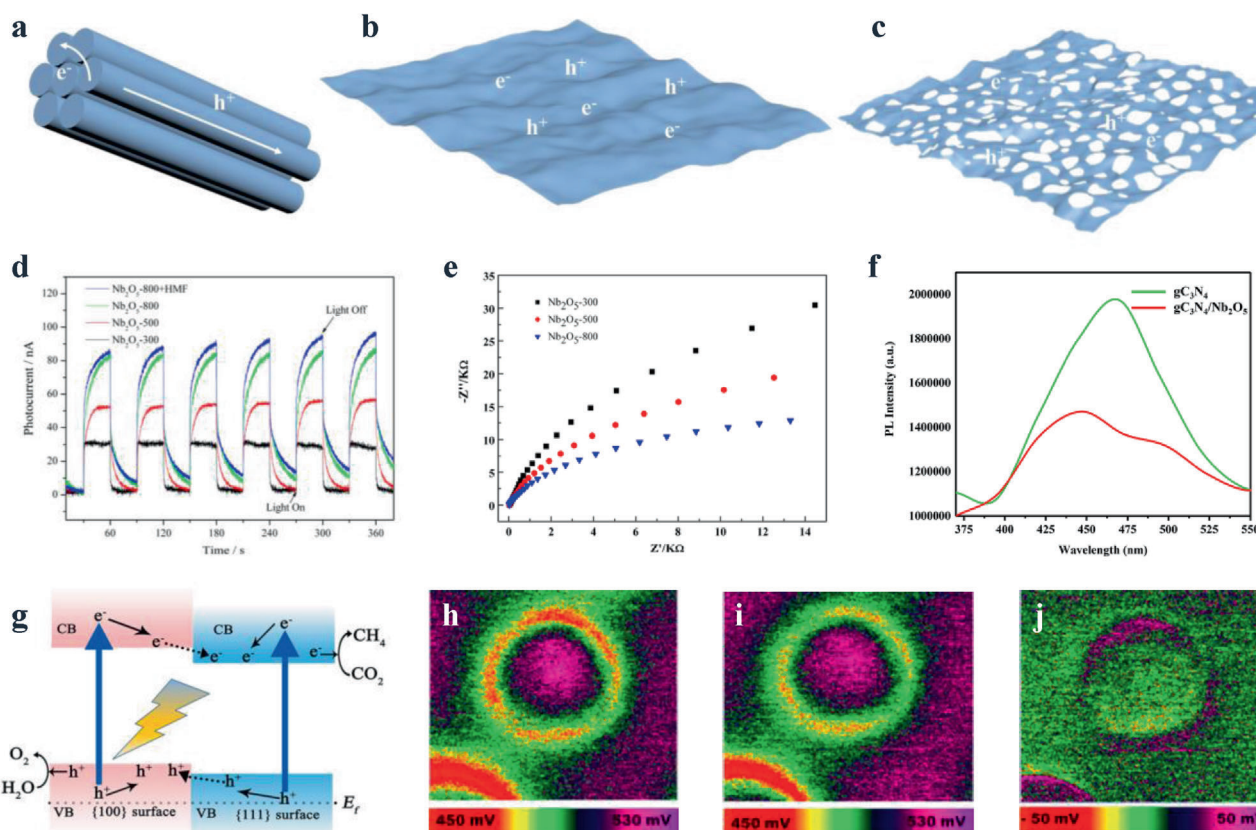
**Figure 8.** a–c) The distribution of charge carriers on different $Nb_2O_5$ catalysts. d) The photocurrent response,[9e] e) electrochemical impedance spectroscopy,[9e] and f) photoluminescence spectroscopy of $Nb_2O_5$-based catalysts.[105b] g) The charge migration on $CeO_2$.[240] SPVM image of $Au/TiO_2$ h) under dark and i) under 532 nm illumination, respectively.[238a] j) The different spectrum from (i) and (h).[238a] d,e) Reproduced with permission.[9e] Copyright 2017, American Chemical Society. f) Reproduced with permission.[105b] Copyright 2019, American Chemical Society. g) Reproduced with permission.[240] Copyright 2015, American Chemical Society. h-j) Reproduced with permission.[239] Copyright 2017, American Chemical Society.

blue and selective oxidation of 5-hydroxymethylfurfural (Table 4, No. 9).[9e,135] For instance, the T-$Nb_2O_5$ obtained by calcination at 800 °C showed the highest photocurrent density than those of counterparts treated at 300 and 500 °C.[9e] Except for the SSA, these results indicated other factors might play an important role in photocatalysis. Previously, the formation energy of oxygen vacancy is changed on different crystalline phases of metal oxide.[236] As revealed by the results of X-ray photoelectron spectra (XPS), a high concentration of oxygen vacancies was observed on H-$Nb_2O_5$.[135] These results suggest the positive effect of oxygen vacancy induced by phase transformation in photocatalysis. The detailed discussion of the role of oxygen vacancy is shown in Section 5.2.

As mentioned above, the photochemical characterizations of catalysts are necessary to reveal the distribution and migration of charge carriers. The photocurrent response, electrochemical impedance spectroscopy (EIS), and photoluminescence spectroscopy (PL) are developed to verify the separation of electrons and holes (Figure 8d–f). Besides, the theoretic calculation was utilized to study the transfer process of excited holes and electrons on metal oxide (Figure 8g).[237,240] Recently, the charge carriers can be directly detected by surface photovoltage microscopy (SPVM).[238] As shown in Figure 8h–j, a circular ring was observed on the differential spectrum of surface photovoltage over

$Au/TiO_2$, which is corresponding to the accumulation of excited holes in the interface (Au–O–Ti) under light irradiation.[239] In principle, these characterization techniques are universal and conducive to the profound understanding of the spatial distribution of charge carriers on $Nb_2O_5$.

## 5.2. The Role of Unsaturated Nb Sites and Oxygen Vacancies

The oxygen vacancies of $Nb_2O_5$ play important roles in the absorption and activation of the substrate.[229,241] Previously, the unsaturated Nb sites were observed with the formation of oxygen vacancies, which were revealed by the results of electron paramagnetic resonance (EPR) and XPS.[229,241] The EPR signal at 2.003 is assigned to the oxygen vacancy.[229] After the adsorption of BA on $HNb_3O_8$ nanosheets, the intensity of the signal at 2.003 was weakened. Meanwhile, the characteristic O–H and C–O bands of BA were shifted to the lower wavenumber in Fourier transform infrared spectra (FT-IR), indicating that the BA molecules were adsorbed on unsaturated Nb sites by the formation of C–O–Nb complex.[229] As a result, the optical absorption edge of BA/$HNb_3O_8$ nanosheets was extended to visible light, indicating that this structure was beneficial for the migration of charge carriers.[229]

**ADVANCED
SCIENCE NEWS**

www.advancedsciencenews.com

**ADVANCED
SCIENCE**
Open Access

www.advancedscience.com

Besides, the unsaturated Nb sites and oxygen vacancies are conducive to the separation of charge carriers.[50c] The HNb$_3$O$_8$ nanosheets with abundant oxygen vacancies exhibited a faster reaction rate and higher separation efficiency of charge carriers than those of urchin-like Nb$_2$O$_5$ and Nb$_2$O$_5$ nanorods, as shown by the results of EIS, photocurrent response.[12c] Meanwhile, PL analysis and time-resolved fluorescence (TRF) results suggested that the oxygen vacancies were conducive to the separation of photogenerated holes and electrons.[77] In addition, the optical absorption ability of catalysts can be affected by the unsaturated Nb sites and oxygen vacancies.[17c,242] The HNb$_3$O$_8$ nanosheets exhibited a wide bandgap (≈3.4 eV), corresponding to the absorption spectrum within 370 nm.[90] With the formation of oxygen vacancies, the bandgap of HNb$_3$O$_8$ nanosheets was narrowed.[50f] Moreover, new energy states with a small bandgap (<0.5 eV) were observed with the increasing concentration of surface unsaturated Nb sites and oxygen vacancies.[17c] This electronic structure can be utilized for the absorption of the full solar spectrum (250–2500 nm).[17c] Thus, heat sourced from the absorption of infrared light over HNb$_3$O$_8$ nanosheets contributed to enhancing reaction rate in kinetics.[17c] The inert C–H bonds of hydrocarbons can be activated by the holes generated at the valence band under UV light irradiation in the thermodynamics.[9a] These results shed light on the balance of electronic structure and concentration of oxygen vacancies for photocatalyst design and preparation.

Especially, the unsaturated Nb sites and oxygen vacancies can be formed without any sacrificial agents under UV light irradiation, indicating that light irradiation can be utilized for the modification of catalyst.[50c] Meanwhile, the concentration of oxygen vacancies was not constant and changed under irradiation.[50c] To reveal the structure of Nb$_2$O$_5$ in situ under light irradiation, theoretical calculations in oxygen-vacancy formation energy on different facets and crystalline phases are necessary for the profound understanding of these phenomena.[9e]

## 5.3. The Role of LAS, BAS, and Acidity

There are consecutive tandem steps involved in photocatalytic processes: 1) light-harvesting on photocatalysts, 2) separation and migration of photogenerated holes and electrons, and 3) succedent surface redox reactions.[243] Particularly, the surface redox reactions and selectivity of products are related to the acid–base properties of photocatalysts.[243] Previously, propene was oxidized to propanal and acetaldehyde on Nb$_2$O$_5$/SiO$_2$ photocatalysts under light irradiation.[233] The selectivity of propanal was much different on the Nb$_2$O$_5$/SiO$_2$ catalysts.[105a] As revealed by results of x-ray absorption near edge structure (XANES) and extended x-ray absorption fine structure (EXAFS), tetrahedral NbO$_4$ and octahedral NbO$_6$ units were present on 0.66 and 4.6 wt% Nb$_2$O$_5$/SiO$_2$, respectively.[233] Notably, the NbO$_6$ octahedra acted as the BAS.[14a] The LAS can be observed with the formation of NbO$_5$ and NbO$_4$ polyhedron.[15] The roles of acid sites are possibly revealed by these results. However, other products, like acetone and acrolein, were also observed, leading to the difficulty in the understanding of the relationship between BAS, LAS, and photooxidation processes.[105a]

After that, the unique acidity of Nb$_2$O$_5$ was found to be instructive to the adsorption–activation process in the photooxidation reaction.[14a,244] The deep oxidation products of alcohols were observed with increasing Lewis acidity of Nb$_2$O$_5$, which may be ascribed to the strong adsorption of aldehydes intermediates on LAS.[228] Besides, the Nb$_2$O$_5$–amide surface complex was generated by the adsorption of amines on Nb$_2$O$_5$.[245] This complex can be excited by light ($\lambda$ > 390 nm) with lower energy than that of Nb$_2$O$_5$.[245] Meanwhile, the yield and selectivity of benzylamine to N-benzylidene benzylamine over commercial Nb$_2$O$_5$ were higher than those over TiO$_2$ under visible light irradiation.[9c] This is mainly due to the activation of amines adsorbed on Nb$_2$O$_5$ via the ligand-to-metal charge transfer (LMCT) transition (**Figure 9**).[245] The electrons transferred from the N 2p orbitals of amides to Nb 4d orbitals of Nb$_2$O$_5$.[244] Then, the $\alpha$-C–H bonds were activated to form the imines.[245] This direct excitation of amines is beneficial to improve the selectivity of the product by inhibiting the generation of other oxygen-containing species, such as ozonide anion radicals (O$^{3-}$) and hydroxyl radicals (HO•).[246] Thus, the undesired deep oxidation was restricted under visible light irradiation.[246] Similarly, alcohols were selectively oxidized to corresponding aldehydes without further oxidation to carboxylic acids.[224] When the surface isolated –OH groups on Nb$_2$O$_5$ were partly removed by a vacuum heat treatment, inert aromatic hydrocarbons with relatively large ionization energy also can be transformed to aldehydes under visible light irradiation (Figure 9).[18] However, the active sites on Nb$_2$O$_5$ are still unclear for the activation of the inert sp$^3$ C–H bond on toluene.[12b,18] Besides, Tsang's group proposed the adsorption–activation process of dyes on Nb$_2$O$_5$.[33a] In their results, Nb$_2$O$_5$ nanorods exhibited higher activity than that of ZnO in the photocatalytic degradation of methylene blue.[33a] After the introduction of a radical scavenger, the comparable activity of Nb$_2$O$_5$ nanorods was observed, indicating that hydroxyl radicals (HO•) played a marginal role in the reaction.[33a] As revealed by FT-IR results, the number of methyl blue molecules adsorbed on Nb$_2$O$_5$ nanorods was higher than that on ZnO, implying that the strong Lewis acidity of Nb$_2$O$_5$ nanorods was beneficial for the adsorption–activation process of methylene blue.[33a]

In addition, the acidity of Nb$_2$O$_5$ is also associated with the selectivity of products in the photoreduction reaction. The photoreduction of CO$_2$ to CH$_4$ was dominated on HNb$_3$O$_8$ nanosheets and SiO$_2$-pillared HNb$_3$O$_8$ that mainly exposed the BAS.[15,221b,c] The yield of CH$_4$ reached 2.9 µmol g$_{cat.}^{-1}$ h$^{-1}$ over SiO$_2$-pillared HNb$_3$O$_8$, which is much higher than that over HNb$_3$O$_8$ (0.47 µmol g$_{cat.}^{-1}$ h$^{-1}$), implying the promoting effects of BAS derived from the dispersed HNb$_3$O$_8$ on SiO$_2$.[220c] Meanwhile, Ribeiro's group found a quite different tendency that improving the number of acid sites on Nb$_2$O$_5$ can promote the photoreduction of CO$_2$ to CO, HCOOH, and CH$_3$COOH.[9b] As shown in Equations (1)–(8) (Section 4.3), protons are vital in the reduction of CO$_2$ to CH$_4$. However, the number of acid sites on different Nb$_2$O$_5$ samples was measured by the ionic-exchange and titration approach, leading to unclear amounts of BASs on the surface of catalysts.[9b] Meanwhile, the activation of CO$_2$ is related to the local structure of Nb–O–Nb.[247] These results lead to an ambiguous understanding of the photoreduction of CO$_2$. Hence, further studies are still necessary to get insight into the relationship between the surface –OH groups, NbO$_x$ units, BAS, LAS, and product selectivity in the photoreduction of CO$_2$.
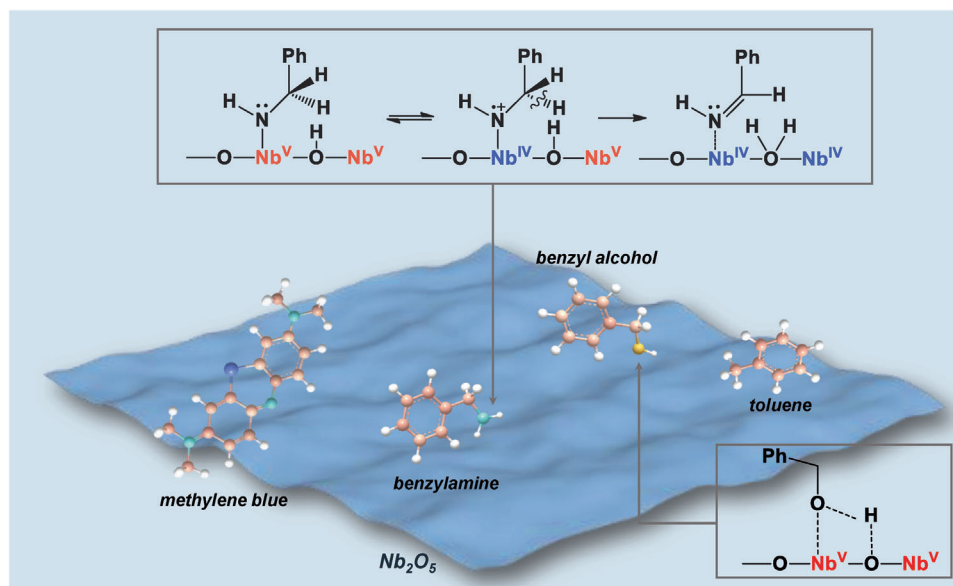
**Figure 9.** The schematic illustration of methylene blue, benzylamine, benzyl alcohol, and toluene adsorbed on $Nb_2O_5$. Adapted with permission.[230] Copyright 2009, American Chemical Society. Adapted with permission.[248] Copyright 2012, American Chemical Society.

### 5.4. The Role of Dopant and Surface Metal Species

The photodegradation of pollutants was observed on doped $Nb_2O_5$ and $M/Nb_2O_5$ catalysts under visible light irradiation (Table 1). The optical absorption ability on doped $Nb_2O_5$ catalysts was revealed by the experimental and theoretical analysis. For instance, an energy level sourced from N 2p orbitals was higher than that of the conduction band of O 2p states in pristine $Nb_2O_5$, leading to low bandgap energy of $N$–$Nb_2O_5$ ($\approx$2.61 eV).[19] In addition, the doping level formed by metal dopants was lower than that of the conduction band on pristine $Nb_2O_5$.[85j,249] Meanwhile, the corresponding energy levels are still competent in the generation of $O_2^{\bullet-}$ species for photodegradation. Furthermore, $Nb_2O_5$ catalysts modified by surface species can be active under visible light irradiation.[171] Zhang's group reported the carbonate modified $Nb_2O_5$ for photodegradation of RhB under visible light irradiation.[171] The $E_g$ of $C$–$Nb_2O_5$ was increased to 3.06 eV after 500 °C calcination, suggesting the carbonaceous species for the enhanced visible-light harvesting.[171] Similar phenomena were also observed in N modified and C, N comodified $Nb_2O_5$.[117,172,173] This can be ascribed to the transfer of electrons from surface $NO_x$ and $CO_x$ species to $Nb_2O_5$ under irradiation, which is analogical of dye-sensitized photocatalysis.[173] For $M/Nb_2O_5$ catalysts, the surface plasmon resonance (SPR) effect of metal species (e.g., Ag, Au, and Cu) is conducive to enhance the response to the visible light irradiation, ascribed to the match between the frequency of the incident light photons and the frequency of surface electrons on metal species.[113a,206,225]

The catalysts structure and properties are also changed by the introduction of dopants on $Nb_2O_5$-based photocatalysts, including the SSA, concentration of oxygen vacancies, and acidity. For instance, the SSA of doped $Nb_2O_5$ catalysts was higher than that of pristine counterpart.[82,85j] These phenomena may be ascribed to the lattice distortion and inhibition of crystal growth by heteroatoms.[82,85j] Besides, the concentration of oxygen va-

cancies can be increased when $Nb_2O_5$ catalysts were doped with N, Zr, Y, Zn, or Mo species.[77,90,184] These phenomena were also observed on other metal oxides, like $Cu$–$CeO_2$.[250] As a result, the photocurrent density of $N$–$Nb_2O_5$ was higher than that of the pristine one.[12b,19] The recombination efficiency of charge carriers is also changed with the concentration of oxygen vacancies, implying an optimal concentration of oxygen vacancies on the $Nb_2O_5$-based photocatalysts in photocatalysis. In the future, machine learning is a promising tool to predict the structure and performance of catalysts.[251]

In addition, the acidity of $Nb_2O_5$-based photocatalysts is also influenced by the dopant and surface metal species. Wolski's group reported $\approx$40% selectivity of dimethoxymethane (DMM) from methanol on $Au/Nb_2O_5$ while <5% selectivity of DMM on $Nb_2O_5$ was observed under UV light irradiation.[225] The DMM is produced by the condensation reaction between the formaldehyde from the oxidation of methanol and adsorbed methanol molecules, implying the significantly decreased acidity of $Nb_2O_5$ after the introduction of the Au species.[225] As revealed by FT-IR results, the number of LASs decreased faster than that of BASs.[225] Meanwhile, the numbers of BASs and LASs were distinct by different preparation approaches.[225] These may be ascribed to the formation of $Nb^{4+}$ species from the reduction of $Nb^{5+}$ in $NbO_4$ units by hydrogen spillover in the reducing atmosphere.[14b,252] Besides, the BAS is possibly neutralized by basic additives in the deposition–precipitation approach.[8c] Occasionally the adsorption of the substrate is enhanced by the dopant on $Nb_2O_5$-based photocatalysts. The adsorption of methylene blue molecules on $Zr$–$Nb_2O_5$ is considerably stronger than that over the pristine counterpart.[77] Similarly, the intact interaction between methyl violet molecules and $Mo$–$Nb_2O_5$ cluster was speculated, as revealed by the results of surface-enhanced Raman scattering (SERS) and first-principles calculation.[90] Furthermore, CO was obtained with a selectivity of 99.5% from the hydrogenation of gaseous $CO_2$ using the small Pd nanocrystals

**ADVANCED
SCIENCE NEWS**

www.advancedsciencenews.com

**ADVANCED
SCIENCE**
Open Access

www.advancedscience.com

supported on $Nb_2O_5$.[253] Density functional theory (DFT) calculations suggested that the Pd(111) facets dominated on the larger nanoparticles were the most favorable sites for methanation of $CO_2$.[253]

### 5.5. The Role of Formed Heterojunctions

Previously, Zheng's group synthesized an amorphous layer on TT-$Nb_2O_5$ microfibers (HN-500).[254] As revealed by the results of VB XPS spectra, the edges of the maximum energy for and TT-$Nb_2O_5$ were identical with that of the amorphous counterpart.[254] Meanwhile, the bandgap of amorphous-phase is ≈0.2 eV higher than that of TT-$Nb_2O_5$, indicating the formation of heterojunction on HN-500.[254] The electronic structure of heterojunction has an advantage in the separation of charge carriers Besides, short-range ordered $Nb_2O_5$ can be dispersed on the surface of amorphous structure, leading to the formation of the interface between amorphous and ordered $Nb_2O_5$.[166] This may be conducive to the desorption of desired products, due to the distinction in acid strength on different phases.[14a]

In addition, the spatial distribution of charge carriers can be observed in other $Nb_2O_5$-based photocatalysts.[255] The type II heterojunctions were obtained by modification of $Nb_2O_5$ with other composites, such as $TiO_2$, $WO_3$, ZnO, CdS, $C_3N_4$, $Ag_3PO_4$, $SrNb_2O_6$, $BiWO_4$, $BiNb_5O_{14}$, and so on.[99e,100b,101a,116,160,162,181,191,205a] For instance, electrons transfer from the CB of $Nb_2O_5$ to the CB of $BiWO_4$ while the holes migrated from the VB of $BiWO_4$ to the VB of $Nb_2O_5$ under UV light irradiation, leading to limited redox potentials of $Nb_2O_5$/$BiWO_4$.[191] When $Nb_2O_5$ was deposited on the $ZnIn_2S_4$, a Z-scheme heterojunction was observed.[217] Partial photogenerated holes and electrons were still present on the VB of $Nb_2O_5$ and CB of $ZnIn_2S_4$, respectively. This electronic structure can maintain the oxidizing potential of $Nb_2O_5$ and reducing the capacity of $ZnIn_2S_4$, respectively.[217] In Z-scheme heterojunction, partial electrons are transferred from the CB of $Nb_2O_5$ to the VB of $ZnIn_2S_4$, which is attributed to photocatalytic performance.[217] Similar heterojunction structures were also observed on Er-$Y_3Al_5O_{12}$@$Nb_2O_5$/Pt/$In_2O_3$ composite catalyst.[214]

Especially, the interface is present in composited $Nb_2O_5$ catalysts.[227] Previously, $Cu_2O$/$Nb_2O_5$ exhibited higher activity than that of the pristine counterpart in the photooxidation of alcohol.[248,256] As revealed by FT-IR results, the adsorption of cyclohexanone over Cu (I) was weaker than that over $Nb^{5+}$ species in the photooxidation of cyclohexanol.[256a] Meanwhile, the oxidative dehydrogenation of alcohols was realized on $Nb^{5+}$ species, indicating the accelerated catalytic recycle on Nb–O–Cu (I) interface.[248] To this end, a series of $Nb_2O_5$-based catalysts have been widely reported in the photocatalytic process. However, few studies focus on the role of the catalyst interface in photocatalysis.

## 6. Summary and Outlook

This review summarized recent advances in the synthesis and application of $Nb_2O_5$-based photocatalysts. Especially, the reaction pathways in the reduction of $CO_2$, oxidation of amines, alcohols, and hydrocarbons are related to the acidity, generated oxygen species, and functional groups on $Nb_2O_5$-based photocatalysts under light irradiation. The understanding greatly relies on the studies in the local structure of $Nb_2O_5$, which is still attractive for researchers, especially in the field of photocatalysis. The universal characterization techniques and photoelectronic properties are the cornerstones to reveal the active sites of $Nb_2O_5$-based photocatalysts.

In the future, $Nb_2O_5$-based photocatalysts are still the potential candidates for the conversion of waste plastics and biomass that are abundant carbon resources. The activations of $sp^3$ C–H bonds and C–C bonds are feasible over $Nb_2O_5$ that exhibits suitable photoredox potentials under light irradiation. Although the yield and selectivity of desired products are limited in the conversion of hydrocarbon and biomass, the reactivity of $Nb_2O_5$ can be further improved by the design of catalyst structure and components. Besides, the local structure and corresponding acidity strength can be in situ controlled on $Nb_2O_5$ under light irradiation. As a result, it is possible to realize the hydrolysis reaction, dehydration reaction, and hydrodeoxygenation reaction under mild conditions. Using the blueprint of photocatalysis, we can improve the conversion of waste plastics and renewable biomass.

Despite the great potential of $Nb_2O_5$-based photocatalysts, the exposed challenges and issues should be considered. The roles of $NbO_4$ and $NbO_6$ units are unclear in photocatalysis, due to the lack of spatiotemporal characterization technique. Apart from that, the studies are insufficient in the interface of Nb–O–metal, which can afford the profound understanding of the adsorption–desorption process and active sites in photocatalysis. Meanwhile, the development of the reactor is conducive to the practical application of the photocatalytic process.[257] Studies in these aspects are necessary for the rational design of $Nb_2O_5$-based photocatalysts. Moreover, novel processes and concepts are urgently required for the large-scale production of $Nb_2O_5$-based photocatalysts.

## Conflict of Interest

The authors declare no conflict of interest.

[1] M. S. Dresselhaus, I. L. Thomas, *Nature* **2001**, *414*, 332.
[2] a) M. Mikkelsen, M. Jorgensen, F. C. Krebs, *Energy Environ. Sci.* **2010**, *3*, 43; b) Z. Zhao, K. Chong, J. Jiang, K. Wilson, X. Zhang, F. Wang, *Renewable Sustainable Energy Rev.* **2018**, *97*, 580.
[3] V. Balzani, A. Credi, M. Venturi, *ChemSusChem* **2008**, *1*, 26.
[4] a) Y. Zhao, X. Zhou, L. Ye, S. C. Tsang, *Nano Rev.* **2012**, *3*, 17631; b) C. Liu, Q. Zhang, W. Hou, Z. Zou, *Sol. RRL* **2020**, *4*, 2000070; c) C. Zhang, F. Wang, *Chin. J. Catal.* **2017**, *38*, 1102.
[5] a) A. Fujishima, K. Honda, *Nature* **1972**, *238*, 37;. b) Q. Wang, K. Domen, *Chem. Rev.* **2019**, *120*, 919.
[6] a) P. Zhang, X. W. D. Lou, *Adv. Mater.* **2019**, *31*, 1900281; b) X. X. Chang, J. L. Gong, *Acta Phys.-Chim. Sin.* **2016**, *32*, 2.
[7] a) N. Luo, T. Montini, J. Zhang, P. Fornasiero, E. Fonda, T. Hou, W. Nie, J. Lu, J. Liu, M. Heggen, L. Lin, C. Ma, M. Wang, F. Fan, S. Jin, F. Wang, *Nat. Energy* **2019**, *4*, 575; b) H. Liu, H. Li, J. Lu, S. Zeng, M. Wang, N. Luo, S. Xu, F. Wang, *ACS Catal.* **2018**, *8*, 4761; c) T. Su, Q. Shao, Z. Qin, Z. Guo, Z. Wu, *ACS Catal.* **2018**, *8*, 2253; d) S. Kampouri, T. N. Nguyen, M. Spodaryk, R. G. Palgrave, A. Züttel, B. Smit, K. C. Stylianou, *Adv. Funct. Mater.* **2018**, *28*, 1806368; e) M. Melchionna, P. Fornasiero, *ACS Catal.* **2020**, *10*, 5493; f) Y. X. Chen, V. Gombac, T. Montini, A. Lavacchi, J. Filippi, H. A. Miller, P. Fornasiero, F. Vizza, *Green Chem.* **2018**, *20*, 2299; g) K. C. Christoforidis, P. Fornasiero, *ChemCatChem* **2017**, *9*, 1523.
[8] a) I. Nowak, M. Ziolek, *Chem. Rev.* **1999**, *99*, 3603;. b) Y. Jing, Y. Xin, Y. Guo, X. Liu, Y. Wang, *Chin. J. Catal.* **2019**, *40*, 1168; c) T. Murayama, M. Haruta, *Chin. J. Catal.* **2016**, *37*, 1694; d) J. Wu, C. Zhou, Y. Zhao, L. Shang, T. Bian, L. Shao, F. Shi, L.-Z. Wu, C.-H. Tung, T. Zhang, *Chin. J. Chem.* **2014**, *32*, 485; e) B. N. Nunes, O. F. Lopes, A. O. T. Patrocinio, D. W. Bahnemann, *Catalysts* **2020**, *10*, 126.
[9] a) X. Jiao, K. Zheng, Q. Chen, X. Li, Y. Li, W. Shao, J. Xu, J. Zhu, Y. Pan, Y. Sun, Y. Xie, *Angew. Chem., Int. Ed.* **2020**, *59*, 15497; b) G. T. S. T. da Silva, A. E. Nogueira, J. A. Oliveira, J. A. Torres, O. F. Lopes, C. Ribeiro, *Appl. Catal., B* **2019**, *242*, 349; c) S. Furukawa, Y. Ohno, T. Shishido, K. Teramura, T. Tanaka, *ACS Catal.* **2011**, *1*, 1150; d) S. Furukawa, T. Shishido, K. Teramura, T. Tanaka, *J. Phys. Chem. C* **2011**, *115*, 19320; e) H. Zhang, Q. Wu, C. Guo, Y. Wu, T. Wu, *ACS Sustainable Chem. Eng.* **2017**, *5*, 3517.
[10] a) C.-s. Guo, M. Li, Z.-g. Liu, D.-l. Zhang, K. Gao, *Chin. Rare Earths* **2014**, *35*, 96; b) H.-R. Fan, K.-F. Yang, F.-F. Hu, S. Liu, K.-Y. Wang, *Geosci. Front.* **2016**, *7*, 335.
[11] a) C. Nico, T. Monteiro, M. P. F. Graça, *Prog. Mater. Sci.* **2016**, *80*, 1; b) B. Niu, Z. Xu, *ChemSusChem* **2019**, *12*, 2819;. c) B. Niu, Z. Xu, *Green Chem.* **2019**, *21*, 874.
[12] a) D. Cao, W. Cai, W. Tao, S. Zhang, D. Wang, D. Huang, *Catal. Lett.* **2017**, *147*, 926; b) K. Su, H. Liu, B. Zeng, Z. Zhang, N. Luo, Z. Huang, Z. Gao, F. Wang, *ACS Catal.* **2020**, *10*, 1324; c) J. Chen, H. Wang, Z. Zhang, L. Han, Y. Zhang, F. Gong, K. Xie, L. Xu, W. Song, S. Wu, *J. Mater. Chem. A* **2019**, *7*, 5493; d) R. Fiz, F. Hernandez-Ramirez, T. Fischer, L. Lopez-Conesa, S. Estrade, F. Peiro, S. Mathur, *J. Phys. Chem. C* **2013**, *117*, 10086; e) R. Brayner, F. Bozon-Verduraz, *Phys. Chem. Chem. Phys.* **2003**, *5*, 1457.
[13] G. T. S. T. da Silva, K. T. G. Carvalho, O. F. Lopes, C. Ribeiro, *Appl. Catal., B* **2017**, *216*, 70.
[14] a) T. Murayama, J. Chen, J. Hirata, K. Matsumoto, W. Ueda, *Catal. Sci. Technol.* **2014**, *4*, 4250; b) K. Nakajima, Y. Baba, R. Noma, M. Kitano, J. N. Kondo, S. Hayashi, M. Hara, *J. Am. Chem. Soc.* **2011**, *133*, 4224;. c) B. Zielinska, M. Arabczyk, R. J. Kalenczuk, *Pol. J. Chem.* **2007**, *81*, 1355.
[15] H. T. Kreissl, M. M. J. Li, Y.-K. Peng, K. Nakagawa, T. J. N. Hooper, J. V. Hanna, A. Shepherd, T.-S. Wu, Y.-L. Soo, S. C. E. Tsang, *J. Am. Chem. Soc.* **2017**, *139*, 12670.
[16] Q. Xia, Z. Chen, Y. Shao, X. Gong, H. Wang, X. Liu, S. F. Parker, X. Han, S. Yang, Y. Wang, *Nat. Commun.* **2016**, *7*, 11162.

[17] a) Z. Liu, W. Dong, J. Wang, C. Dong, Y. Lin, I. W. Chen, F. Huang, *iScience* **2020**, *23*, 100767;. b) W. Zhao, W. Zhao, G. Zhu, T. Lin, F. Xu, F. Huang, *Dalton Trans.* **2016**, *45*, 3888;. c) M.-Q. Yang, L. Shen, Y. Lu, S. W. Chee, X. Lu, X. Chi, Z. Chen, Q.-H. Xu, U. Mirsaidov, G. W. Ho, *Angew. Chem., Int. Ed.* **2018**, *58*, 3077; d) H. Cui, G. Zhu, Y. Xie, W. Zhao, C. Yang, T. Lin, H. Gu, F. Huang, *J. Mater. Chem. A* **2015**, *3*, 11830.
[18] K. Tamai, K. Murakami, S. Hosokawa, H. Asakura, K. Teramura, T. Tanaka, *J. Phys. Chem. C* **2017**, *121*, 22854.
[19] H. Huang, C. Wang, J. Huang, X. Wang, Y. Du, P. Yang, *Nanoscale* **2014**, *6*, 7274.
[20] X. Chen, T. Yu, X. Fan, H. Zhang, Z. Li, J. Ye, Z. Zou, *Appl. Surf. Sci.* **2007**, *253*, 8500.
[21] a) M. J. Enright, K. Gilbert-Bass, B. Sarsito, B. M. Cossairt, *Chem. Mater.* **2019**, *31*, 2677; b) S. Dhawan, T. Dhawan, A. G. Vedeshwar, *Mater. Lett.* **2014**, *126*, 32.
[22] M. Rooth, A. Johansson, M. Boman, A. Hårsta, *Mater. Res. Soc. Symp. Proc.* **2005**, *901*, 0901.
[23] a) Y. Kobayashi, H. Hata, T. E. Mallouk, *Mater. Res. Soc. Symp. Proc.* **2006**, *988*, 0988; b) Y. Kobayashi, H. Hata, M. Salama, T. E. Mallouk, *Nano Lett.* **2007**, *7*, 2142; c) S. Lee, K. Teshima, Y. Niina, S. Suzuki, K. Yubuta, T. Shishido, M. Endo, S. Oishi, *CrystEngComm* **2009**, *11*, 2326.
[24] C. Yan, D. Xue, *Adv. Mater.* **2008**, *20*, 1055.
[25] F. E. I. Liu, D. Xue, *Mod. Phys. Lett. B* **2009**, *23*, 3769.
[26] X. Han, Q. Kuang, M. Jin, Z. Xie, L. Zheng, *J. Am. Chem. Soc.* **2009**, *131*, 3152.
[27] X. Liu, R. Yuan, Y. Liu, S. Zhu, J. Lin, X. Chen, *New J. Chem.* **2016**, *40*, 6276.
[28] W. Merchan-Merchan, M. Farmahini Farahani, *Mater. Chem. Phys.* **2013**, *140*, 516.
[29] P. P. George, V. G. Pol, A. Gedanken, *Nanoscale Res. Lett.* **2007**, *2*, 17.
[30] a) L. Li, J. Deng, J. Chen, X. Sun, R. Yu, G. Liu, X. Xing, *Chem. Mater.* **2009**, *21*, 1207; b) L. Li, J. Deng, R. Yu, J. Chen, X. Wang, X. Xing, *Inorg. Chem.* **2010**, *49*, 1397.
[31] C. Y. Xu, Y. Z. Liu, L. Zhen, *Ceram. Int.* **2012**, *38*, 861.
[32] W. Hu, Z. Liu, D. Tian, S. Zhang, Y. Zhao, J. Yao, *J. Wuhan Univ. Technol.* **2009**, *24*, 245.
[33] a) Y. Zhao, C. Eley, J. Hu, J. S. Foord, L. Ye, H. He, S. C. Tsang, *Angew. Chem., Int. Ed.* **2012**, *51*, 3846; b) M. Qamar, M. Abdalwadoud, M. I. Ahmed, A. M. Azad, B. Merzougui, S. Bukola, Z. H. Yamani, M. N. Siddiqui, *ACS Appl. Mater. Interfaces* **2015**, *7*, 17954; c) X. Liu, G. Liu, H. Chen, J. Ma, R. Zhang, *J. Phys. Chem. Solids* **2017**, *111*, 8; d) G. K. Ong, C. A. Saez Cabezas, M. N. Dominguez, S. L. Skjærvø, S. Heo, D. J. Milliron, *Chem. Mater.* **2019**, *32*, 468.
[34] a) Y. Zhou, Z. Qiu, M. Lü, A. Zhang, Q. Ma, *J. Lumin.* **2008**, *128*, 1369; b) H. Wen, Z. Liu, J. Wang, Q. Yang, Y. Li, J. Yu, *Appl. Surf. Sci.* **2011**, *257*, 10084; c) L. Du, Z. Long, H. Wen, W. Ge, Y. Zhou, J. Wang, *CrystEngComm* **2014**, *16*, 9096; d) W.-F. Rao, Y. Zhang, Z. Wang, Q. Yu, Y. Yang, *Mater. Lett.* **2018**, *211*, 168; e) C. Singh, M. K. Pandey, A. M. Biradar, A. K. Srivastava, G. Sumana, *RSC Adv.* **2014**, *4*, 15458.
[35] H. Luo, M. Wei, K. Wei, *J. Nanomater.* **2009**, *2009*, 758353.
[36] A. Le Viet, R. Jose, S. Ramakrishna, *Mater. Res. Soc. Symp. Proc.* **2009**, *1240*, 1240.
[37] a) J. He, Z. Wang, S. Yang, Y. Hu, D. Guo, *Fine Chem.* **2015**, *32*, 658; b) J. H. Kang, Y. Myung, J. W. Choi, D. M. Jang, C. W. Lee, J. Park, E. H. Cha, *J. Mater. Chem.* **2012**, *22*, 8413; c) J. H. Lim, J. Choi, *J. Ind. Eng. Chem.* **2009**, *15*, 860.
[38] X. Wang, Q. Li, L. Zhang, Z. Hu, L. Yu, T. Jiang, C. Lu, C. Yan, J. Sun, Z. Liu, *Adv. Mater.* **2018**, *30*, 1800963.
[39] H. Zhang, Y. Wang, P. Liu, S. L. Chou, J. Z. Wang, H. Liu, G. Wang, H. Zhao, *ACS Nano* **2015**, *10*, 507.

[40] a) K. Saito, A. Kudo, *Bull. Chem. Soc. Jpn.* **2009**, *82*, 1030; b) K. Saito, A. Kudo, *Dalton Trans.* **2013**, *42*, 6867.

[41] A. Le Viet, R. Jose, M. V. Reddy, B. V. R. Chowdari, S. Ramakrishna, *J. Phys. Chem. C* **2010**, *114*, 21795.

[42] M. Mozetič, U. Cvelbar, M. K. Sunkara, S. Vaddiraju, *Adv. Mater.* **2005**, *17*, 2138.

[43] K. Nakagawa, T. Jia, W. Zheng, S. M. Fairclough, M. Katoh, S. Sugiyama, S. C. Tsang, *Chem. Commun.* **2014**, *50*, 13702.

[44] H. Luo, M. Wei, K. Wei, *Mater. Chem. Phys.* **2010**, *120*, 6.

[45] a) L. Wang, B. Ruan, J. Xu, H. K. Liu, J. Ma, *RSC Adv.* **2015**, *5*, 36104; b) Z. Y. Jia, M. N. Liu, X. L. Zhao, X. S. Wang, Z. H. Pan, Y. G. Zhang, *Acta Phys.-Chim. Sin.* **2017**, *33*, 2510.

[46] H. Li, Y. Zhu, S. Dong, L. Shen, Z. Chen, X. Zhang, G. Yu, *Chem. Mater.* **2016**, *28*, 5753.

[47] W. Fan, Q. Zhang, W. Deng, Y. Wang, *Chem. Mater.* **2013**, *25*, 3277.

[48] S. H. Lee, B. J. Kim, T. Nasir, I. J. Choi, B. J. Jeong, C. Woo, H. K. Lim, Y. Kim, S. S. Nanda, D. K. Yi, H. K. Yu, J. Y. Choi, *Nanotechnology* **2020**, *31*, 315502.

[49] M. Liu, C. Yan, Y. Zhang, *Sci. Rep.* **2015**, *5*, 8326.

[50] a) N. Lee, Y.-M. Chung, *Appl. Surf. Sci.* **2016**, *370*, 160; b) J. Park, J.-H. Lee, Y.-M. Chung, Y.-W. Suh, *Adv. Powder Technol.* **2017**, *28*, 2524; c) L. Shen, Y. Xia, S. Lin, S. Liang, L. Wu, *Nanoscale* **2017**, *9*, 14654; d) S. Uchida, N. Zettsu, K. Hirata, K. Kami, K. Teshima, *RSC Adv.* **2016**, *6*, 67514; e) M. Zarei-Chaleshtori, M. Hosseini, R. Edalatpour, S. M. S. Masud, R. R. Chianelli, *Microchem. J.* **2013**, *110*, 361; f) Y. Zhou, T. Wen, W. Kong, B. Yang, Y. Wang, *Dalton Trans.* **2017**, *46*, 13854.

[51] P. Wen, L. Ai, T. Liu, D. Hu, F. Yao, *Mater. Des.* **2017**, *117*, 346.

[52] S. Takenaka, S. Miyake, S. Uwai, H. Matsune, M. Kishida, *J. Phys. Chem. C* **2015**, *119*, 12445.

[53] H. Huang, G. Zhao, N. Zhang, K. Sun, *Nanoscale* **2019**, *11*, 16222.

[54] L. Wang, X. Bi, S. Yang, *Adv. Mater.* **2016**, *28*, 7672.

[55] D. M. Antonelli, J. Y. Ying, *Angew. Chem., Int. Ed.* **1996**, *35*, 426.

[56] P. D. Yang, D. Y. Zhao, D. I. Margolese, B. F. Chmelka, G. D. Stucky, *Nature* **1998**, *396*, 152.

[57] a) L. Ye, S. Xie, B. Yue, L. Qian, S. Feng, S. C. Tsang, Y. Li, H. He, *CrystEngComm* **2010**, *12*, 344; b) B. Lee, D. Lu, J. N. Kondo, K. Domen, *J. Am. Chem. Soc.* **2002**, *124*, 11256.

[58] K. Brezesinski, J. Wang, J. Haetge, C. Reitz, S. O. Steinmueller, S. H. Tolbert, B. M. Smarsly, B. Dunn, T. Brezesinski, *J. Am. Chem. Soc.* **2010**, *132*, 6982.

[59] K. Nakajima, T. Fukui, H. Kato, M. Kitano, J. N. Kondo, S. Hayashi, M. Hara, *Chem. Mater.* **2010**, *22*, 3332.

[60] A. Serrà, R. Artal, J. García-Amorós, B. Sepúlveda, E. Gómez, J. Nogués, L. Philippe, *Adv. Sci.* **2020**, *7*, 1902447.

[61] T. J. Novakowski, J. K. Tripathi, G. M. Hosinski, G. Joseph, A. Hassanein, *Appl. Surf. Sci.* **2016**, *362*, 35.

[62] G.-Z. Li, H.-P. Tang, W.-Y. Zhang, G. Li, L.-L. Yu, Y.-N. Li, *Rare Met.* **2013**, *34*, 77.

[63] a) R. Abdul Rani, A. S. Zoolfakar, M. F. Mohamad Ryeeshyam, A. S. Ismail, M. H. Mamat, S. Alrokayan, H. Khan, K. Kalantar-zadeh, M. R. Mahmood, *J. Electron. Mater.* **2019**, *48*, 3805; b) N. Alias, S. A. Rosli, Z. Hussain, T. W. Kian, A. Matsuda, Z. Lockman, *Mater. Today: Proc.* **2019**, *17*, 1033; c) K. Kim, M.-S. Kim, P.-R. Cha, S. H. Kang, J.-H. Kim, *Chem. Mater.* **2016**, *28*, 1453; d) M. M. Rahman, R. A. Rani, A. Z. Sadek, A. S. Zoolfakar, M. R. Field, T. Ramireddy, K. Kalantar-zadeh, Y. Chen, *J. Mater. Chem. A* **2013**, *1*, 11019.

[64] M. Ristić, S. Popović, S. Musić, *Mater. Lett.* **2004**, *58*, 2658.

[65] a) F. Hashemzadeh, R. Rahimi, A. Ghaffarinejad, *Ceram. Int.* **2014**, *40*, 9817; b) J. C. Rooke, T. Barakat, J. Brunet, Y. Li, M. F. Finol, J.-F. Lamonier, J.-M. Giraudon, R. Cousin, S. Siffert, B. L. Su, *Appl. Catal., B* **2015**, *162*, 300.

[66] S. Li, C. N. Schmidt, Q. Xu, X. Cao, G. Cao, *ChemNanoMat* **2016**, *2*, 675.

[67] I. Nowak, M. Jaroniec, *Top. Catal.* **2008**, *49*, 193.

[68] R. Shao, Z. Cao, Y. Xiao, H. Dong, W. He, Y. Gao, J. Liu, *RSC Adv.* **2014**, *4*, 26447.

[69] Y.-H. Pai, S.-Y. Fang, *J. Power Sources* **2013**, *230*, 321.

[70] H. Kominami, K. Oki, M. Kohno, S.-i. Onoue, Y. Kera, B. Ohtani, *J. Mater. Chem.* **2001**, *11*, 604.

[71] a) R. Rathnasamy, P. Thangasamy, V. Aravindhan, P. Sathyanarayanan, V. Alagan, *Res. Chem. Intermed.* **2019**, *45*, 3571; b) R. Panetta, A. Latini, I. Pettiti, C. Cavallo, *Mater. Chem. Phys.* **2017**, *202*, 289; c) S. Parraud, L. G. Hubert-Pfalzgraf, H. Floch, *Mater. Res. Soc. Symp. Proc.* **1990**, *180*, 397.

[72] J. Ge, F. Wang, Z. Xu, X. Shen, C. Gao, D. Wang, G. Hu, J. Gu, T. Tang, J. Wei, *J. Mater. Chem. B* **2020**, *8*, 2618.

[73] L. D. Gómez, J. E. Rodríguez-Páez, *Nano-Struct. Nano-Objects* **2019**, *17*, 43.

[74] C. D. Gomez, J. E. Rodriguez-Paez, *Process. Appl. Ceram.* **2018**, *12*, 218.

[75] Y. Tao, B. Singh, V. Jindal, Z. Tang, P. P. Pescarmona, *Green Chem.* **2019**, *21*, 5852.

[76] T. Tsuzuki, P. G. McCormick, *Mater. Trans.* **2001**, *42*, 1623.

[77] B. Boruah, R. Gupta, J. M. Modak, G. Madras, *Nanoscale Adv.* **2019**, *1*, 2748.

[78] J.-Y. Liang, C.-H. Wu, Y. Zheng, P. Shen, S.-Y. Chen, *Appl. Phys. A* **2013**, *115*, 1429.

[79] a) J. Wu, J. Li, X. Lü, L. Zhang, J. Yao, F. Zhang, F. Huang, F. Xu, *J. Mater. Chem.* **2010**, *20*, 1942; b) G. Liu, B. Jin, K. Bao, H. Xie, J. Guo, X. Ji, R. Zhang, Q. Jiang, *Int. J. Hydrogen Energy* **2017**, *42*, 6065; c) Y. Yoo, Y. C. Kang, *J. Alloys Compd.* **2019**, *776*, 722.

[80] L. Kong, C. Zhang, J. Wang, W. Qiao, L. Ling, D. Long, *Sci. Rep.* **2016**, *6*, 21177.

[81] R. Asahi, T. Morikawa, T. Ohwaki, K. Aoki, Y. Taga, *Science* **2001**, *293*, 269.

[82] a) S. Ding, R. Wang, Z. Zhang, S. Qiu, *Chem. J. Chin. Univ.* **2014**, *35*, 695; b) S. Ding, R. Wang, P. Zhang, B. Kang, D. Zhang, Z. Zhang, S. Qiu, *Chem. Res. Chin. Univ.* **2018**, *34*, 274.

[83] a) A. K. Kulkarni, R. P. Panmand, Y. A. Sethi, S. R. Kadam, S. P. Tekale, G. H. Baeg, A. V. Ghule, B. B. Kale, *Int. J. Hydrogen Energy* **2018**, *43*, 19873; b) S. Hemmati, G. Li, X. Wang, Y. Ding, Y. Pei, A. Yu, Z. Chen, *Nano Energy* **2019**, *56*, 118.

[84] A. K. Kulkarni, C. S. Praveen, Y. A. Sethi, R. P. Panmand, S. S. Arbuj, S. D. Naik, A. V. Ghule, B. B. Kale, *Dalton Trans.* **2017**, *46*, 14859.

[85] a) F. T. Aquino, J. L. Ferrari, S. J. L. Ribeiro, A. Ferrier, P. Goldner, R. R. Gonçalves, *Opt. Mater.* **2013**, *35*, 387; b) F. T. Aquino, R. R. Pereira, J. L. Ferrari, S. J. L. Ribeiro, A. Ferrier, P. Goldner, R. R. Gonçalves, *Mater. Chem. Phys.* **2014**, *147*, 751; c) F. T. Aquino, J. L. Ferrari, L. J. Q. Maia, S. J. L. Ribeiro, A. Ferrier, P. Goldner, R. R. Gonçalves, *J. Lumin.* **2016**, *170*, 431; d) F. J. Caixeta, F. T. Aquino, R. R. Pereira, R. R. Gonçalves, *J. Lumin.* **2016**, *171*, 63; e) R. R. Pereira, F. T. Aquino, A. Ferrier, P. Goldner, R. R. Gonçalves, *J. Lumin.* **2016**, *170*, 707; f) F. T. Aquino, F. J. Caixeta, K. de Oliveira Lima, M. Kochanowicz, D. Dorosz, R. R. Gonçalves, *J. Lumin.* **2018**, *199*, 138; g) W. C. Muscelli, F. T. Aquino, F. J. Caixeta, L. R. R. Nunes, L. Zur, M. Ferrari, R. R. Gonçalves, *J. Lumin.* **2018**, *199*, 454; h) A. Esteves, L. C. A. Oliveira, T. C. Ramalho, M. Goncalves, A. S. Anastacio, H. W. P. Carvalho, *Catal. Commun.* **2008**, *10*, 330; i) N. P.de Moraes, M. L. C. P. da Silva, L. A. Rodrigues, *Mater. Lett.* **2018**, *228*, 486; j) J. A. Oliveira, M. O. Reis, M. S. Pires, L. A. M. Ruotolo, T. C. Ramalho, C. R. Oliveira, L. C. T. Lacerda, F. G. E. Nogueira, *Mater. Chem. Phys.* **2019**, *228*, 160.

[86] C. Hu, W. Y. Teoh, S. Ji, C. Ye, A. Iwase, *AIChE J.* **2016**, *62*, 352.

[87] B. Hu, Y. Liu, *J. Alloys Compd.* **2015**, *635*, 1.

[88] X. Wang, G. Chen, C. Zhou, Y. Yu, G. Wang, *Eur. J. Inorg. Chem.* **2012**, *2012*, 1742;

[89] D. Ni, H. Jiang, H. Gong, T. Su, *Chin. J. Rare Met.* **2016**, *40*, 43.

[90] Y. Peng, C. Lin, M. Tang, L. Yang, Y. Yang, J. Liu, Z. Huang, Z. Li, *Appl. Surf. Sci.* **2020**, *509*, 145376.

[91] a) P. Li, Z. Xiong, S. Zhu, M. Wang, Y. Hu, H. Gu, Y. Wang, W. Chen, *Int. J. Hydrogen Energy* **2017**, *42*, 30186; b) T. Kawano, H. Kakemoto, H. Irie, *Mater. Lett.* **2015**, *156*, 94.

[92] a) J. Bai, J. Xue, R. Wang, Z. Zhang, S. Qiu, *Dalton Trans.* **2018**, *47*, 3400;. b) T. Goswami, K. M. Reddy, A. Bheemaraju, *ChemistrySelect* **2019**, *4*, 6790; c) Y. Xin, L. Dong, Y. Guo, X. Liu, Y. Hu, Y. Wang, *J. Catal.* **2019**, *375*, 202; d) K. Murata, D. Kosuge, J. Ohyama, Y. Mahara, Y. Yamamoto, S. Arai, A. Satsuma, *ACS Catal.* **2020**, *10*, 1381; e) K. An, S. Alayoglu, N. Musselwhite, K. Na, G. A. Somorjai, *J. Am. Chem. Soc.* **2014**, *136*, 6830.

[93] a) L. Dong, Y. Xin, X. Liu, Y. Guo, C.-W. Pao, J.-L. Chen, Y. Wang, *Green Chem.* **2019**, *21*, 3081; b) K. Kon, W. Onodera, S. Takakusagi, K.-i. Shimizu, *Catal. Sci. Technol.* **2014**, *4*, 3705; c) K. A. Resende, F. B. Noronha, C. E. Hori, *Renewable Energy* **2020**, *149*, 198; d) Y. Xin, Y. Jing, L. Dong, X. Liu, Y. Guo, Y. Wang, *Chem. Commun.* **2019**, *55*, 9391; e) Y. Shao, Q. Xia, X. Liu, G. Lu, Y. Wang, *ChemSusChem* **2015**, *8*, 1761;. f) J. C. Serrano-Ruiz, J. A. Dumesic, *ChemSusChem* **2009**, *2*, 581.

[94] a) F. Du, X. Jin, W. Yan, M. Zhao, P. S. Thapa, R. V. Chaudhari, *Catal. Today* **2018**, *302*, 227; b) R. Brayner, G. Viau, G. M. da Cruz, F. Fiévet-Vincent, F. Fiévet, F. Bozon-Verduraz, *Catal. Today* **2000**, *57*, 187.

[95] a) R. Brayner, D. dos Santos Cunha, F. Bozon-Verduraz, *Catal. Today* **2003**, *78*, 419; b) H.-Y. Lin, H.-C. Yang, W.-L. Wang, *Catal. Today* **2011**, *174*, 106; c) W.-J. Chen, X. Sun, Y. Liu, M. Huang, W. Xu, X. Pan, Q. Wu, Z. Yi, *ACS Appl. Nano Mater.* **2020**, *3*, 2573.

[96] E. A. Kyriakidou, O. S. Alexeev, A. P. Wong, C. Papadimitriou, M. D. Amiridis, J. R. Regalbuto, *J. Catal.* **2016**, *344*, 749.

[97] a) S. Furukawa, T. Shishido, K. Teramura, T. Tanaka, *ACS Catal.* **2012**, *2*, 175; b) L. C. A. Oliveira, H. S. Oliveira, G. Mayrink, H. S. Mansur, A. A. P. Mansur, R. L. Moreira, *Appl. Catal., B* **2014**, *152*, 403; c) Y. A. Bhembe, L. P. Lukhele, S. Sinha Ray, L. N. Dlamini, *Dalton Trans.* **2020**, *49*, 7474;. d) T. Su, R. Peng, Z. D. Hood, M. Naguib, I. N. Ivanov, J. K. Keum, Z. Qin, Z. Guo, Z. Wu, *ChemSusChem* **2018**, *11*, 688;. e) H. Huang, J. Zhou, J. Zhou, M. Zhu, *Catal. Sci. Technol.* **2019**, *9*, 3373.

[98] S. Yoshida, T. Tanaka, T. Hanada, T. Hiraiwa, H. Kanai, T. Funabiki, *Catal. Lett.* **1992**, *12*, 277.

[99] a) A. L. da Silva, D. N. F. Muche, S. Dey, D. Hotza, R. H. R. Castro, *Ceram. Int.* **2016**, *42*, 5113; b) T. A. Sedneva, E. P. Lokshin, M. L. Belikov, A. T. Belyaevskii, *Inorg. Mater.* **2013**, *49*, 382; c) M. S. Jeon, T. K. Lee, D. H. Kim, H. Joo, H. T. Kim, *Sol. Energy Mater. Sol. Cells* **1999**, *57*, 217; d) H.-Y. Lin, H.-C. Huang, W.-L. Wang, *Microporous Mesoporous Mater.* **2008**, *115*, 568; e) S.-M. Lam, J.-C. Sin, I. Satoshi, A. Z. Abdullah, A. R. Mohamed, *Appl. Catal., A* **2014**, *471*, 126; f) K. T. G. Carvalho, A. E. Nogueira, O. F. Lopes, G. Byzynski, C. Ribeiro, *Ceram. Int.* **2017**, *43*, 3521; g) Q.-Z. Huang, J.-C. Wang, P.-P. Wang, H.-C. Yao, Z.-J. Li, *Int. J. Hydrogen Energy* **2017**, *42*, 6683; h) M. Wang, H. Wang, Y. Ren, C. Wang, Z. Weng, B. Yue, H. He, *Nanomaterials* **2018**, *8*, 427.

[100] a) V. S. Santana, N. R. C. Fernandes Machado, *Catal. Today* **2008**, *133–135*, 606; b) J. Xing, Z. Shan, K. Li, J. Bian, X. Lin, W. Wang, F. Huang, *J. Phys. Chem. Solids* **2007**, *69*, 23; c) T. K. Ghorai, S. Sikdar, S. Das, S. Pathak, S. Pattanayak, N. Biswas, *Mater. Today: Proc.* **2018**, *5*, 9760.

[101] a) S. S. Arbuj, R. R. Hawaldar, U. P. Mulik, D. P. Amalnerkar, *J. Nanoeng. Nanomanuf.* **2013**, *3*, 79; b) D. M. Tobaldi, A. Sever Skapin, R. C. Pullar, M. P. Seabra, J. A. Labrincha, *Ceram. Int.* **2013**, *39*, 2619; c) Z. T. Omran, N. Y. Fairooz, *Int. J. ChemTech Res.* **2016**, *9*, 149.

[102] a) O. Sacco, J. J. Murcia, A. E. Lara, M. Hernandez-Laverde, H. Rojas, J. A. Navio, M. C. Hidalgo, V. Vaiano, *Mater. Sci. Semicond. Process.* **2020**, *107*, 104839; b) H. S. Park, J. W. Ko, W. B. Ko, *Asian J. Chem.* **2016**, *28*, 2769.

[103] a) F. V.de Andrade, G. M. de Lima, R. Augusti, M. G. Coelho, Y. P. Q. Assis, I. R. M. Machado, *J. Environ. Chem. Eng.* **2014**, *2*, 2352; b) Z. Yue, A. Liu, C. Zhang, J. Huang, M. Zhu, Y. Du, P. Yang, *Appl. Catal., B* **2017**, *201*, 202.

[104] a) G. Pereira da Costa, R. A. Rafael, J. C. S. Soares, A. B. Gaspar, *Catal. Today* **2020**, *344*, 240; b) S. G. Ghugal, S. S. Umare, R. Sasikala, *RSC Adv.* **2016**, *6*, 64047.

[105] a) T. Tanaka, H. Nojima, H. Yoshida, H. Nakagawa, T. Funabiki, S. Yoshida, *Catal. Today* **1993**, *16*, 297; b) I. Khan, N. Baig, A. Qurashi, *ACS Appl. Energy Mater.* **2019**, *2*, 607.

[106] F. Huang, H. Zhao, A. Yan, Z. Li, H. Liang, Q. Gao, Y. Qiang, *J. Alloys Compd.* **2017**, *695*, 489.

[107] T. Zhao, S. Shen, X. Liu, Y. Guo, C.-W. Pao, J.-L. Chen, Y. Wang, *Catal. Sci. Technol.* **2019**, *9*, 4002.

[108] A. M. Ferrari-Lima, R. G. Marques, M. L. Gimenes, N. R. C. Fernandes-Machado, *Catal. Today* **2015**, *254*, 119.

[109] a) W. Li, R. Gao, M. Chen, S. Zhou, L. Wu, *J. Colloid Interface Sci.* **2013**, *411*, 220;. b) K. C. Devarayapalli, S. V. Prabhakar Vattikuti, T. V. Madhukar Sreekanth, P. Chidananndha Nagajyothi, J. Shim, *ChemistrySelect* **2019**, *4*, 13250; c) S. D. Khairnar, M. R. Patil, V. S. Shrivastava, *Iran. J. Catal.* **2018**, *8*, 143; d) X. Kong, Q. Lu, J. Huang, L. Li, J. Zhang, X. Wang, J. Li, Y. Wang, Q. Feng, *J. Alloys Compd.* **2018**, *746*, 68; e) O. F. Lopes, E. C. Paris, C. Ribeiro, *Appl. Catal., B* **2014**, *144*, 800; f) S. Zarrin, F. Heshmatpour, *J. Phys. Chem. Solids* **2020**, *140*, 109271.

[110] a) R. Ullah, H. Sun, H. M. Ang, M. O. Tadé, S. Wang, *Ind. Eng. Chem. Res.* **2013**, *52*, 3320; b) S.-M. Lam, J.-C. Sin, A. R. Mohamed, *Mater. Lett.* **2016**, *167*, 141.

[111] a) N. P. Ferraz, F. C. F. Marcos, A. E. Nogueira, A. S. Martins, M. R. V. Lanza, E. M. Assaf, Y. J. O. Asencios, *Mater. Chem. Phys.* **2017**, *198*, 331; b) I. L. O. Brasileiro, V. S. Madeira, C. P. de Souza, A. L. Lopes-Moriyama, M. L. R. de Almeida Ramalho, *J. Photochem. Photobiol., A* **2019**, *388*, 112199.

[112] J. Chen, H. Wang, G. Huang, Z. Zhang, L. Han, W. Song, M. Li, Y. Zhang, *J. Alloys Compd.* **2017**, *728*, 19.

[113] a) R. G. Marques, A. M. Ferrari-Lima, V. Slusarski-Santana, N. R. C. Fernandes-Machado, *J. Environ. Manage.* **2017**, *195*, 242;. b) R. P. Souza, T. K. F. S. Freitas, F. S. Domingues, O. Pezoti, E. Ambrosio, A. M. Ferrari-Lima, J. C. Garcia, *J. Photochem. Photobiol., A* **2016**, *329*, 9; c) F. S. Domingues, H. C. L. Geraldino, T. K. F. de Souza Freitas, C. A. de Almeida, F. F. de Figueiredo, J. C. Garcia, *Environ. Technol.* **2019**, 1.

[114] S. Zhang, B. Zhang, D. Chen, Z. Guo, M. Ruan, Z. Liu, *Nano Energy* **2021**, *79*, 105485.

[115] Z. Huang, Z. Zhao, C. Zhang, J. Lu, H. Liu, N. Luo, J. Zhang, F. Wang, *Nat. Catal.* **2020**, *3*, 170.

[116] Y. Hong, C. Li, G. Zhang, Y. Meng, B. Yin, Y. Zhao, W. Shi, *Chem. Eng. J.* **2016**, *299*, 74.

[117] Y. Wen, S. Liu, Y. Zhang, Z. Yang, A. Zhu, X. Du, *Mater. Lett.* **2016**, *165*, 156.

[118] H. Cui, K. Dwight, S. Soled, A. Wold, *J. Solid State Chem.* **1995**, *115*, 187.

[119] J. Yang, J. Hao, S. Xu, J. Dai, Y. Wang, X. Pang, *Chem. Eng. J.* **2018**, *353*, 100.

[120] N. P. de Moraes, F. A. Torezin, G. V. Juca Dantas, J. G. M. de Sousa, R. B. Valim, R. da Silva Rocha, R. Landers, M. L. C. P. da Silva, L. A. Rodrigues, *Ceram. Int.* **2020**, *46*, 14505.

[121] C. Martin, I. Martin, V. Rives, G. Solana, V. Loddo, L. Palmisano, A. Sclafani, *J. Mater. Sci.* **1997**, *32*, 6039.

[122] N. P. Ferraz, A. E. Nogueira, F. C. F. Marcos, V. A. Machado, R. R. Rocca, E. M. Assaf, Y. J. O. Asencios, *Rare Met.* **2020**, *39*, 230.

[123] C. Karunakaran, R. Dhanalakshmi, *Cent. Eur. J. Chem.* **2009**, *7*, 134.

[124] C. Karunakaran, R. Dhanalakshmi, *Radiat. Phys. Chem.* **2009**, *78*, 8.

[125] C. Karunakaran, R. Dhanalakshmi, P. Gomathisankar, G. Manikandan, *J. Hazard. Mater.* **2010**, *176*, 799.

**ADVANCED
SCIENCE NEWS**

www.advancedsciencenews.com

**ADVANCED
SCIENCE**
Open Access

www.advancedscience.com

[126] L. Kong, C. Wang, H. Zheng, X. Zhang, Y. Liu, *J. Phys. Chem. C* **2015**, *119*, 16623.

[127] R. R. M. Silva, J. A. Oliveira, L. A. M. Ruotolo, A. L. A. Faria, C. Ribeiro, F. G. E. Nogueira, *Mater. Lett.* **2020**, *273*, 127915.

[128] T. Mano, S. Nishimoto, Y. Kameshima, M. Miyake, *Chem. Eng. J.* **2015**, *264*, 221.

[129] F. Houshang, H. Fatemeh, R. Rahmatollah, G. Ali, *J. Cluster Sci.* **2014**, *25*, 651.

[130] H. Sudrajat, S. Babel, J. Phanthuwongpakdee, T. K. Nguyen, *J. Alloys Compd.* **2019**, *806*, 543.

[131] I. F. B. Silva, A. R. Martins, K. Krambrock, M. G. Rosmaninho, I. Binatti, F. C. C. Moura, *J. Photochem. Photobiol., A* **2020**, *388*, 112168.

[132] A. G. S. Prado, L. B. Bolzon, C. P. Pedroso, A. O. Moura, L. L. Costa, *Appl. Catal., B* **2008**, *82*, 219.

[133] A. G. S. Prado, E. A. Faria, J. R. SouzaDe, J. D. Torres, *J. Mol. Catal. A: Chem.* **2005**, *237*, 115.

[134] N. Suzuki, T. Athar, Y.-T. Huang, K. Shimasaki, N. Miyamoto, Y. Yamauchi, *J. Ceram. Soc. Jpn.* **2011**, *119*, 405.

[135] N. Kumari, K. Gaurav, S. K. Samdarshi, A. S. Bhattacharyya, S. Paul, B. Rajbongshi, K. Mohanty, *Sol. Energy Mater. Sol. Cells* **2020**, *208*, 110408.

[136] N. T. do Prado, L. C. A. Oliveira, *Appl. Catal., B* **2017**, *205*, 481.

[137] S. Kajita, F. Mimuro, T. Yoshida, N. Ohno, N. Yoshida, *ChemPhysChem* **2018**, *19*, 3237.

[138] Z. Wang, G. Tong, J. He, S. Yang, Y. Hu, *Mater. Rev.* **2015**, *29*, 1.

[139] M. Danish, A. Pandey, *J. Mater. Sci.: Mater. Electron.* **2016**, *27*, 6939.

[140] G. Falk, M. Borlaf, M. J. Lopez-Munoz, J. C. Farinas, J. B. Rodrigues Neto, R. Moreno, *J. Mater. Res.* **2017**, *32*, 3271.

[141] X. Liu, R. Zheng, R. Yuan, L. Peng, Y. Liu, J. Lin, *ECS J. Solid State Sci. Technol.* **2017**, *6*, P665.

[142] F. Nakagomi, S. E. Cerruti, M. R. de Freitas, E. S. Freitas Neto, F. V. de Andrade, G. O. Siqueira, *Chem. Phys. Lett.* **2019**, *729*, 37.

[143] S. Nishimoto, T. Takiguchi, Y. Kameshima, M. Miyake, *Chem. Phys. Lett.* **2019**, *726*, 34.

[144] F. F. Brites-Nobrega, I. A. Lacerda, S. V. Santos, C. C. Amorim, V. S. Santana, N. R. C. Fernandes-Machado, J. D. Ardisson, A. B. Henriques, M. M. D. Leao, *Catal. Today* **2015**, *240*, 168.

[145] C. D. Gomez, J. E. Rodriguez-Paez, *Coatings* **2015**, *5*, 511.

[146] N. P. de Moraes, G. C. Neves, F. A. Torezin, M. L. C. P. da Silva, L. A. Rodrigues, *Inorg. Chem. Commun.* **2018**, *98*, 145.

[147] N. Perciani de Moraes, R. Bacani, M. L. C. Pinto da Silva, T. M. B. Campos, G. P. Thim, L. A. Rodrigues, *Ceram. Int.* **2018**, *44*, 6645.

[148] N. P. de Moraes, L. A. Bacetto, L. K. Paiva, G. S. dos Santos, M. L. C. P. da Silva, L. A. Rodrigues, *J. Sol-Gel Sci. Technol.* **2019**, *89*, 571.

[149] N. P. de Moraes, R. B. Anselmo, L. O. Sartor, G. V. J. Dantas, L. A. Rodrigues, L. Chaguri e Carvalho, *Mater. Lett.* **2020**, *273*, 127932.

[150] H. S. Park, W. B. Ko, *Elastomers Compos.* **2014**, *49*, 330.

[151] B. Gao, J. Fu, K. Huo, W. Zhang, Y. Xie, P. K. Chu, *J. Am. Ceram. Soc.* **2011**, *94*, 2330.

[152] S. Zarrin, F. Heshmatpour, *J. Hazard. Mater.* **2018**, *351*, 147.

[153] H. Miyazaki, H. Matsui, T. Kuwamoto, S. Ito, S. Karuppuchamy, M. Yoshihara, *Microporous Mesoporous Mater.* **2009**, *118*, 518.

[154] Y. Shen, T. Xiong, J. Shang, K. Yang, *Res. Chem. Intermed.* **2008**, *34*, 353.

[155] Z. Zhang, J. Zhang, C. Yue, J. Hu, S. Zheng, *Micro Nano Lett.* **2018**, *13*, 175.

[156] H. Liu, N. Gao, M. Liao, X. Fang, *Sci. Rep.* **2015**, *5*, 7716.

[157] S. Qi, R. Zuo, Y. Liu, Y. Wang, *Mater. Res. Bull.* **2013**, *48*, 1213.

[158] M. Vosoughifar, *J. Mater. Sci.: Mater. Electron.* **2017**, *28*, 532.

[159] A. J. dos Santos, L. M. B. Batista, C. A. Martinez-Huitle, A. Paula de Melo Alves, S. Garcia-Segura, *Catalysts* **2019**, *9*, 1070.

[160] R. Shao, X. Zeng, Z. Cao, H. Dong, L. Wang, F. Wang, J. Liu, Z. Li, Q. Liang, *RSC Adv.* **2015**, *5*, 102101.

[161] S. Qi, L. Fei, R. Zuo, Y. Wang, Y. Wu, *J. Mater. Chem. A* **2014**, *2*, 8190.

[162] J.-C. Xing, J.-J. Bian, J.-H. Yang, F.-Q. Huang, *J. Inorg. Mater.* **2007**, *22*, 927.

[163] F. Hashemzadeh, R. Rahimi, A. Gaffarinejad, V. Jalalat, S. Safapour, *Desalin. Water Treat.* **2015**, *56*, 181.

[164] A. M. Raba, J. Barba-Ortega, M. R. Joya, *Appl. Phys. A* **2015**, *119*, 923.

[165] C. Jaramillo-Paez, F. J. Sanchez-Fernandez, J. A. Navio, M. C. Hidalgo, *J. Photochem. Photobiol., A* **2018**, *359*, 40.

[166] P. Zhang, M. Wang, J. Wang, X. Teng, S. Zhang, H. Xie, S. Ding, *J. Non-Cryst. Solids* **2018**, *500*, 371.

[167] S.-q. Guo, X. Zhang, Z. Zhou, G.-d. Gao, L. Liu, *J. Mater. Chem. A* **2014**, *2*, 9236.

[168] F. Hashemzadeh, R. Rahimi, A. Gaffarinejad, *Environ. Sci. Pollut. Res.* **2014**, *21*, 5121.

[169] W. Dong, F. Pan, Y. Wang, S. Xiao, K. Wu, G. Q. Xu, W. Chen, *Appl. Surf. Sci.* **2017**, *392*, 514.

[170] L. Wolski, A. Walkowiak, M. Ziolek, *Mater. Res. Bull.* **2019**, *118*, 110530.

[171] S. Ge, H. Jia, H. Zhao, Z. Zheng, L. Zhang, *J. Mater. Chem.* **2010**, *20*, 3052.

[172] J. Xue, R. Wang, Z. Zhang, S. Qiu, *Dalton Trans.* **2016**, *45*, 16519.

[173] F. A. Qaraah, S. A. Mahyoub, M. E. Hafez, G. Xiu, *RSC Adv.* **2019**, *9*, 39561.

[174] X. Li, N. Kikugawa, J. Ye, *Chem. - Eur. J.* **2009**, *15*, 3538.

[175] Q. Dai, B. Yuan, M. Guo, K. Zhang, X. Chen, Z. Song, T. T. Nguyen, X. Wang, S. Lin, J. Fan, Y. Li, H. Liu, Z. Guo, *Ceram. Int.* **2020**, *46*, 13210.

[176] X. Li, N. Kikugawa, J. Ye, *Adv. Mater.* **2008**, *20*, 3816.

[177] G. Ramanjaneya Reddy, K. Chennakesavulu, *J. Mol. Struct.* **2014**, *1075*, 406.

[178] X. Liu, W. Que, X. Xing, Y. Yang, X. Yin, J. Shao, *RSC Adv.* **2016**, *6*, 9581.

[179] X. Qu, M. Liu, Z. Gao, H. Zhai, W. Ren, L. Shi, F. Du, *Appl. Surf. Sci.* **2019**, *506*, 144688.

[180] Z. Xu, J. Jiang, Q. Zhang, G. Chen, L. Zhou, L. Li, *J. Colloid Interface Sci.* **2020**, *563*, 131.

[181] Y. Huang, L. Mi, X. Liu, S. Bi, H. J. Seo, *J. Lumin.* **2019**, *207*, 149.

[182] H. Wang, P. Xu, T. Wang, *Thin Solid Films* **2001**, *388*, 68.

[183] Y. Zhang, H. Zhao, X. Zhao, J. Lin, N. Li, Z. Huo, Z. Yan, M. Zhang, S. Hu, *Sci. China Mater.* **2019**, *62*, 203.

[184] J. Xue, R. Wang, Z. Zhang, S. Qiu, *Chem. J. Chin. Univ.* **2018**, *39*, 319.

[185] V. K. Mahajan, S. P. Patil, S. H. Sonawane, G. H. Sonawane, *AIMS Biophys.* **2016**, *3*, 415.

[186] D. C. Castro, R. P. Cavalcante, J. Jorge, M. A. U. Martines, L. C. S. Oliveira, G. A. Casagrande, A. Machulek, *J. Braz. Chem. Soc.* **2016**, *27*, 303.

[187] M. Z. Fidelis, E. Abreu, O. A. A. Dos Santos, E. S. Chaves, R. Brackmann, D. T. Dias, G. G. Lenzi, *Catalysts* **2019**, *9*, 343.

[188] E. Hass Caetano Lacerda, F. C. Monteiro, J. R. Kloss, S. T. Fujiwara, *J. Photochem. Photobiol., A* **2020**, *388*, 112084.

[189] F. F. de Brites-Nobrega, A. N. B. Polo, A. M. Benedetti, M. M. D. Leao, V. Slusarski-Santana, N. R. C. Fernandes-Machado, *J. Hazard. Mater.* **2013**, *263*, 61.

[190] G. Huang, J. Chen, D. Wang, Y. Sun, L. Jiang, Y. Yu, J. Zhou, S. Ma, Y. Kang, *Mater. Lett.* **2016**, *173*, 227.

[191] J. Wu, J. Li, J. Liu, J. Bai, L. Yang, *RSC Adv.* **2017**, *7*, 51046.

[192] S. D. Marathe, V. S. Shrivastava, *Desalin. Water Treat.* **2016**, *57*, 4652.

[193] M. K. Silva, R. G. Marques, N. R. C. F. Machado, O. A. A. Santos, *Braz. J. Chem. Eng.* **2002**, *19*, 359.

[194] F. F. Brites, V. S. Santana, N. R. C. Fernandes-Machado, *Top. Catal.* **2011**, *54*, 264.

[195] Y.-H. Chin, J.-C. Sin, S.-M. Lam, *Mater. Lett.* **2018**, *216*, 8.

[196] Y.-H. Chin, J.-C. Sin, S.-M. Lam, A. R. Mohamed, *J. Mater. Sci.: Mater. Electron.* **2019**, *30*, 1739.

[197] A. M. Ferrari-Lima, R. G. Marques, N. R. C. Fernandes-Machado, M. L. Gimenes, *Catal. Today* **2013**, *209*, 79.

[198] Y. Du, S. Zhang, J. Wang, J. Wu, H. Dai, *J. Environ. Sci.* **2018**, *66*, 358.

[199] Y. Du, X. Wang, J. Wu, C. Qi, Y. Li, *Particuology* **2018**, *40*, 123.

[200] T. G. Josue, L. N. B. Almeida, M. F. Lopes, O. A. A. Santos, G. G. Lenzi, *J. Environ. Manage.* **2020**, *268*, 110711.

[201] A. E. Nogueira, O. F. Lopes, A. B. S. Neto, C. Ribeiro, *Chem. Eng. J.* **2017**, *312*, 220.

[202] Y. A. Bhembe, L. N. Dlamini, *J. Environ. Sci. Health, Part A: Toxic/Hazard. Subst. Environ. Eng.* **2020**, *55*, 1003.

[203] L. A. Morais, C. Adan, A. S. Araujo, A. P. M. A. Guedes, J. Marugan, *J. Adv. Oxid. Technol.* **2016**, *19*, 256.

[204] A. Dessì, M. Monai, M. Bessi, T. Montini, M. Calamante, A. Mordini, G. Reginato, C. Trono, P. Fornasiero, L. Zani, *ChemSusChem* **2018**, *11*, 793.

[205] a) K. K. Mandari, N. Son, S. Pandey, Y. S. Kim, G. A. K. M. Rafiqul Bari, M. Kang, *J. Alloys Compd.* **2020**, *835*, 155399; b) C. Zhou, R. Shi, G. Yang, X. Meng, L. Z. Wu, C. H. Tung, T. Zhang, *Mater. Today Chem.* **2018**, *10*, 259; c) L. Li, J. Deng, R. Yu, J. Chen, Z. Wang, X. Xing, *J. Mater. Chem. A* **2013**, *1*, 11894; d) F. Idrees, R. Dillert, D. Bahnemann, F. K. Butt, M. Tahir, *Catalysts* **2019**, *9*, 169.

[206] X. Lang, X. Chen, J. Zhao, *Chem. Soc. Rev.* **2014**, *43*, 473.

[207] T. Takata, J. Jiang, Y. Sakata, M. Nakabayashi, N. Shibata, V. Nandal, K. Seki, T. Hisatomi, K. Domen, *Nature* **2020**, *581*, 411.

[208] T. Sreethawong, S. Ngamsinlapasathian, S. H. Lim, S. Yoshikawa, *Chem. Eng. J.* **2013**, *215–216*, 322.

[209] X. Ma, Y. Chen, H. Li, X. Cui, Y. Lin, *Mater. Res. Bull.* **2015**, *66*, 51.

[210] S. Y. Moon, B. Naik, K. An, S. M. Kim, J. Y. Park, *RSC Adv.* **2016**, *6*, 18198.

[211] H. Zhang, Q. Lin, S. Ning, Y. Zhou, H. Lin, J. Long, Z. Zhang, X. Wang, *RSC Adv.* **2016**, *6*, 96809.

[212] W. Hong, Y. Zhou, C. Lv, Z. Han, G. Chen, *ACS Sustainable Chem. Eng.* **2018**, *6*, 889.

[213] J. Yan, G. Wu, N. Guan, L. Li, *Appl. Catal., B* **2014**, *152–153*, 280.

[214] D. Wang, X. Wang, J. Liu, M. Zhang, Y. Song, Z. Zhang, J. Wang, *Mater. Sci. Eng., B* **2020**, *257*, 114549.

[215] M. I. Ghouri, E. Ahmed, *Ceram. Int.* **2019**, *45*, 23196.

[216] Z. Yue, D. Chu, H. Huang, J. Huang, P. Yang, Y. Du, M. Zhu, C. Lu, *RSC Adv.* **2015**, *5*, 47117.

[217] Y. Wang, X. Kong, M. Jiang, F. Zhang, X. Lei, *Inorg. Chem. Front.* **2020**, *7*, 437.

[218] W. Zhou, K. Cheng, J. Kang, C. Zhou, V. Subramanian, Q. Zhang, Y. Wang, *Chem. Soc. Rev.* **2019**, *48*, 3193.

[219] S. Xie, Q. Zhang, G. Liu, Y. Wang, *Chem. Commun.* **2016**, *52*, 35.

[220] a) H. Wang, J. Jia, L. Wang, K. Butler, R. Song, G. Casillas, L. He, N. P. Kherani, D. D. Perovic, L. Jing, A. Walsh, R. Dittmeyer, G. A. Ozin, *Adv. Sci.* **2019**, *6*, 1902170; b) X. Li, H. Pan, W. Li, Z. Zhuang, *Appl. Catal., A* **2012**, *413–414*, 103; c) X. Li, W. Li, Z. Zhuang, Y. Zhong, Q. Li, L. Wang, *J. Phys. Chem. C* **2012**, *116*, 16047.

[221] K.-N. Hu, W.-M. Yau, R. Tycko, *J. Am. Chem. Soc.* **2010**, *132*, 24.

[222] a) M. Wang, M. Liu, J. Lu, F. Wang, *Nat. Commun.* **2020**, *11*, 1083;. b) H. Yang, D. Yang, X. Wang, *Angew. Chem., Int. Ed.* **2020**, *59*, 15527.

[223] J.-Y. Li, Y.-H. Li, M.-Y. Qi, Q. Lin, Z.-R. Tang, Y.-J. Xu, *ACS Catal.* **2020**, *10*, 6262.

[224] S. Furukawa, T. Shishido, K. Teramura, T. Tanaka, *ChemPhysChem* **2014**, *15*, 2665.

[225] L. Wolski, M. El-Roz, M. Daturi, G. Nowaczyk, M. Ziolek, *Appl. Catal., B* **2019**, *258*, 117978.

[226] F. Liu, Y. Wang, X. Kong, D. Lei, F. Zhang, X. Lei, *RSC Adv.* **2019**, *9*, 6177.

[227] G. S. G. De Carvalho, L. H. Chagas, C. G. Fonseca, P. P. de Castro, A. C. SantAna, A. A. Leitao, G. W. Amarante, *New J. Chem.* **2019**, *43*, 5863.

[228] T. Ohuchi, T. Miyatake, Y. Hitomi, T. Tanaka, *Catal. Today* **2007**, *120*, 233.

[229] S. Liang, L. Wen, S. Lin, J. Bi, P. Feng, X. Fu, L. Wu, *Angew. Chem., Int. Ed.* **2014**, *53*, 2951.

[230] T. Shishido, T. Miyatake, K. Teramura, Y. Hitomi, H. Yamashita, T. Tanaka, *J. Phys. Chem. C* **2009**, *113*, 18713.

[231] J. Dai, Q. Sun, X. Fan, M. Lu, *Fine Chem.* **2014**, *31*, 1480.

[232] T. Tsunehiro, F. Sakae, T. Takuzo, Y. Satohiro, *Chem. Lett.* **1994**, *23*, 809.

[233] S. Yoshida, Y. Nishimura, T. Tanaka, H. Kanai, T. Funabiki, *Catal. Today* **1990**, *8*, 67.

[234] K. Yubuta, K. Teshima, S. Oishi, *Surf. Interface Anal.* **2014**, *46*, 957.

[235] Y. Bai, Y. Zhou, J. Zhang, X. Chen, Y. Zhang, J. Liu, J. Wang, F. Wang, C. Chen, C. Li, R. Li, C. Li, *ACS Catal.* **2019**, *9*, 3242.

[236] Z. Zhang, Y. Wang, M. Wang, J. Lü, L. Li, Z. Zhang, M. Li, J. Jiang, F. Wang, *Chin. J. Catal.* **2015**, *36*, 1623.

[237] R. Li, H. Han, F. Zhang, D. Wang, C. Li, *Energy Environ. Sci.* **2014**, *7*, 1369;

[238] a) R. Chen, S. Pang, H. An, J. Zhu, S. Ye, Y. Gao, F. Fan, C. Li, *Nat. Energy* **2018**, *3*, 655; b) R. Chen, F. Fan, T. Dittrich, C. Li, *Chem. Soc. Rev.* **2018**, *47*, 8238.

[239] S. Wang, Y. Gao, S. Miao, T. Liu, L. Mu, R. Li, F. Fan, C. Li, *J. Am. Chem. Soc.* **2017**, *139*, 11771.

[240] P. Li, Y. Zhou, Z. Zhao, Q. Xu, X. Wang, M. Xiao, Z. Zou, *J. Am. Chem. Soc.* **2015**, *137*, 9547.

[241] W. Bi, C. Ye, C. Xiao, W. Tong, X. Zhang, W. Shao, Y. Xie, *Small* **2014**, *10*, 2820.

[242] Z. Yu, E. R. Waclawik, Z. Wang, X. Gu, Y. Yuan, Z. Zheng, *J. Mater. Chem. A* **2017**, *5*, 4607.

[243] X. Li, J. Yu, M. Jaroniec, *Chem. Soc. Rev.* **2016**, *45*, 2603.

[244] T. Shishido, K. Teramura, T. Tanaka, *Catal. Sci. Technol.* **2011**, *1*, 541.

[245] S. Furukawa, Y. Ohno, T. Shishido, K. Teramura, T. Tanaka, *J. Phys. Chem. C* **2012**, *117*, 442.

[246] S. Furukawa, T. Shishido, K. Teramura, T. Tanaka, *ACS Catal.* **2011**, *2*, 175.

[247] T. Hou, N. Luo, Y.-T. Cui, J. Lu, L. Li, K. E. MacArthur, M. Heggen, R. Chen, F. Fan, W. Tian, S. Jin, F. Wang, *Appl. Catal., B* **2019**, *245*, 262.

[248] S. Furukawa, D. Tsukio, T. Shishido, K. Teramura, T. Tanaka, *J. Phys. Chem. C* **2012**, *116*, 12181.

[249] T. S. El-Shazly, W. M. I. Hassan, S. T. Abdel Rahim, N. K. Allam, *Int. J. Hydrogen Energy* **2015**, *40*, 13867.

[250] M. Wang, M. Shen, X. Jin, J. Tian, M. Li, Y. Zhou, L. Zhang, Y. Li, J. Shi, *ACS Catal.* **2019**, *9*, 4573.

[251] M. Zhong, K. Tran, Y. Min, C. Wang, Z. Wang, C.-T. Dinh, P. De Luna, Z. Yu, A. S. Rasouli, P. Brodersen, S. Sun, O. Voznyy, C.-S. Tan, M. Askerka, F. Che, M. Liu, A. Seifitokaldani, Y. Pang, S.-C. Lo, A. Ip, Z. Ulissi, E. H. Sargent, *Nature* **2020**, *581*, 178.

[252] J. Jia, D. D. Perovic, P. G. O'Brien, T. Fei, L. M. Reyes, T. E. Burrow, Y. Dong, K. Liao, G. A. Ozin, L. He, Q. Qiao, M. Varela, S. J. Pennycook, M. Hmadeh, A. S. Helmy, N. P. Kherani, *Adv. Sci.* **2016**, *3*, 1600189.

[253] J. Jia, P. Li, K. K. Ghuman, C. Qiu, Z.-H. Lu, C. V. Singh, N. P. Kherani, D. D. Perovic, H. Wang, M. Ghoussoub, Z. Zheng, L. Wang, A. A. Jelle, Y. Dong, C. Qian, Y. Shao, G. A. Ozin, Z. Lu, A. Gu, T. Wood, P. G. O'Brien, P. Duchesne, P. Zhang, Q. Qiao, Y. Zhu, Q. Qiao, Q. Wang, M. Ye, A. S. Helmy, N. P. Kherani, *Adv. Sci.* **2017**, *4*, 1700252.

[254] Y. Zhang, L. Pei, Z. Zheng, Y. Yuan, T. Xie, J. Yang, S. Chen, J. Wang, E. R. Waclawik, H. Zhu, *J. Mater. Chem. A* **2015**, *3*, 18045.

[255] a) X. Xu, L. Hu, N. Gao, S. Liu, S. Wageh, A. A. Al-Ghamdi, A. Al-shahrie, X. Fang, *Adv. Funct. Mater.* **2015**, *25*, 445; b) L. Zheng, S. Han, H. Liu, P. Yu, X. Fang, *Small* **2016**, *12*, 1527.

[256] a) S. Furukawa, Y. Ohno, T. Shishido, K. Teramura, T. Tanaka, *ChemPhysChem* **2011**, *12*, 2823;. b) S. Furukawa, A. Tamura, T. Shishido, K. Teramura, T. Tanaka, *Appl. Catal., B* **2011**, *110*, 216.

[257] L. Zhang, Z. Zhu, B. Liu, C. Li, Y. Yu, S. Tao, T. Li, *Adv. Sci.* **2019**, *6*, 1900583.

**2003156 (24 of 25)**

**Kaiyi Su** received his B.S. degree from the China University of Petroleum-Beijing (2015). Currently, he is a Ph.D. student under the supervision of Prof. Feng Wang at the Dalian Institute of Chemical Physics, the Chinese Academy of Sciences. His research interests include the design and synthesis of metal oxides and heterogeneous photocatalysis.



**Paolo Fornasiero** received a degree in chemistry at the University of Trieste (1992) and a Ph.D. degree in heterogeneous catalysis (1997). He is the scientific responsible of the CNR Research Unit located at the University of Trieste - Department of Chemical and Pharmaceutical Sciences, associated with the Institute of Chemistry of OrganoMetallic Compounds (ICCOM) of Florence. The scientific interests of Prof. Fornasiero are in the field of inorganic chemistry, with attention to the design and development of multifunctional metal–oxide nanosystems for their advanced applications in energy-related material science and environmental heterogeneous catalysis.



**Feng Wang** received his B.S. degree at Zhengzhou University (1999) and Ph.D. degree at the Dalian Institute of Chemical Physics (DICP), the Chinese Academy of Sciences (2005). He serves as a professor and a group leader at DICP (2009), a joint professor in the State Key Laboratory of Catalysis (2013), and has been the director of the Division of Biomass Conversion and Bio-Energy at DICP since 2018. The current research interests of Prof. Wang include heterogeneous catalysis, biomass conversion, and life cycle analysis.